NUMERICAL INVESTIGATION OF A DC GLOW DISCHARGE IN AN ARGON GAS: TWO-COMPONENT PLASMA MODEL

A THESIS SUBMITTED TO
THE GRADUATE SCHOOL OF NATURAL AND APPLIED SCIENCES
OF
MIDDLE EAST TECHNICAL UNIVERSITY

BY

EFE HASAN KEMANECİ

IN PARTIAL FULFILLMENT OF THE REQUIREMENTS
FOR
THE DEGREE OF MASTER OF SCIENCE
IN
PHYSICS

SEPTEMBER 2009

Approval of the thesis:

NUMERICAL INVESTIGATION OF A DC GLOW DISCHARGE IN AN ARGON GAS: TWO-COMPONENT PLASMA MODEL

submitted by **EFE HASAN KEMANECİ** in partial fulfillment of the requirements for the degree of **Master of Science in Physics Department, Middle East Technical University** by,

Prof. Dr. Canan Özgen _____
Dean, Graduate School of **Natural and Applied Sciences**

Prof. Dr. Sinan Bilikmen _____
Head of Department, **Physics**

Asst. Prof. Dr. İsmail Rafatov _____
Supervisor, **Physics Department, METU**

Examining Committee Members:

Assoc. Prof. Dr. Serhat Çakır
Physics Department, METU _____

Asst. Prof. Dr. İsmail Rafatov
Physics Department, METU _____

Dr. Ali Alaçakır
SANAEM, TAEK _____

Dr. Demiral Akbar
Physics Department, METU _____

Dr. Burak Yedierler
Physics Department, METU _____

Date: **09.09.2009**

I hereby declare that all information in this document has been obtained and presented in accordance with academic rules and ethical conduct. I also declare that, as required by these rules and conduct, I have fully cited and referenced all material and results that are not original to this work.

Name, Last Name: EFE HASAN KEMANECİ

Signature :

ABSTRACT

NUMERICAL INVESTIGATION OF A DC GLOW DISCHARGE IN AN ARGON GAS: TWO-COMPONENT PLASMA MODEL

Kemaneci, Efe Hasan

M.S., Department of Physics

Supervisor : Asst. Prof. Dr. İsmail Rafatov

September 2009, 66 pages

This thesis deals with a one and two dimensional numerical modeling of a low-pressure DC glow discharge in argon gas. We develop two-component fluid model which uses the diffusion-drift theory for the gas discharge plasma and consists of continuity equations for electrons and ions, as well as Poisson equation for electric field. Numerical method is based on the control volume technique. Calculations are carried out in MATLAB environment. Computed results are compared with the classic theory of glow discharges and available experimental data.

Keywords: glow discharge, numerical investigation, two-component plasma model, control volume method, argon

ÖZ

DOĞRU AKIM IŞILTILI DEŞARJ ÖZELLİKLERİNİN NUMERİK ARAŞTIRILMASI:
İKİ BİLEŞENLİ PLAZMA MODELİ

Kemaneci, Efe Hasan
Yüksek Lisans, Fizik Bölümü
Tez Yöneticisi : Yard. Doç İsmail Rafatov

Eylül 2009, 66 sayfa

Bu tezde argon gazındaki doğru akım, düşük basınç ışıltılı deşarjın bir ve iki boyuttaki nümerik modellemesi incelenecektir. Gaz deşarjını difüzyon sürüklenme teorisi ile açıklayan ve elektron ve iyon süreklilik eşitliklerinin yanında Elektrik alan için Poisson eşitliğini içeren iki bileşenli akışkan modeli şekillendirilmiştir. Nümerik metod olarak kontrol hacim tekniği kullanılmıştır. Hesaplamalar MATLAB programı ile yapılmıştır. Sonuçlar ışıltılı deşarjın klasik teorisi ve mevcut deneysel verilerle karşılaştırılmıştır.

Anahtar Kelimeler: ışıltılı deşarj, nümerik çözüm, iki bileşenli plazma modeli, kontrol hacim tekniği, argon

to my lovely family...

ACKNOWLEDGMENTS

I would like to thank to my supervisor Asst. Prof. Dr. İsmail Rafatov, for his encouragement and perceptiveness. Without his guidance, this work would be very hard to accomplish.

I want to thank chairperson Prof. Dr. Sinan Bilikmen, Dr. Demiral Akbar, Mrs. Sevim Aygar, Mrs. Zeynep Eke and Mrs. Gülşen Özdemir Parlak for their help during my study. Additionally, I thank to Assoc. Prof. Dr. Bayram Tekin, Prof. Dr. Atalay Karasu, Dr. İnanç Kanık, Dr. Barış Malcıoğlu , Nazım Duğan and Tahsin Çağrı Şişman for their assist in my graduate years.

I also want to thank to Murat Mesta, Sinan Değer, Taylan Takan, to all fellow assistants in my department, Eralp Erman, METU Aikido dojo members for having spent invaluable moments all together and to Buket Kaleli for her endless support during the process.

I would like to thank to Scientific and Technical Research Council of Turkey (TUBITAK) for financial support during my study.

TABLE OF CONTENTS

LIST OF TABLES

TABLES

LIST OF FIGURES

FIGURES

CHAPTER 1

INTRODUCTION

1.1 Historical Perspective

Though many kinds of discharges were observed in the nature (e.g. lightning as spark, Aurora Borealis as glow discharge) since the dawn of mankind, the term "gas discharge" dates back to 1600, with the observation of the fact that friction-charged insulated conductors lose charge. Charles-Augustin de Coulomb was the first scientist experimentally showing in 1785 that the charge leaks through the air. Afterwards, the improvements in the power generators lead to the discovery of arc discharge in 1803 by V. V. Petrov. Later in the same century Faraday discovered and studied the glow discharge. Additional improvements in the tube materials and vacuum chambers allowed the study of various forms of discharges. The studies in this area was important in J. J. Thomson's work that leads to discovery of electron and the measurement of the charge mass ratio. Moreover it leads to the discovery of mass spectroscopy by J. J. Thomson and F. W. Aston. Later the curtains hiding the secrets in the discharge physics started to draw back with the help of Atomic physics and Quantum physics. The process is understood to be the ionizations and excitations in the gas leaded mainly by electron flow. J. S. E. Townsend was the founder of the basics of the discharge physics which is now used in the modern physics, chemistry and many areas. Nowadays it is possible to observe the use of discharge types in spectroscopy, sputtering processes, plasma physics, laser applications etc. and even in everyday life as street advertisements, conventional and energy saving lambs, plasma panels etc. [1] [2] [8] [9].

1.2 Basics

Gas discharge originates from the discharge of a capacitor in a closed circuit. At sufficiently high voltages, the capacitor starts to leak electrical current leading short-cut in the circuit. Later on any flow of charges in a gas is called discharge. Normally in a gas state we do no observe any conductivity, except the lightnings etc which occur in rare specific conditions. However, at some values of pressure and voltage difference, gas breakdown occurs and the matter starts to allow current flow through it. The mostly observed example in nature is the lightning. The clouds and ground behave like two electrodes, and when the voltage is sufficiently high, the gas allows the passage of electrons by emitting light, caused by the excitations of air molecules or atoms. Similarly, electrons and ions move through the gas and interact with the atoms in the laboratory resulting excitations and ionization.

Basically a cylindrical tube with electrodes at the ends is used in the experiments. The gas in the tube becomes conductor at some specific voltage applied to the electrodes. The process can be carried out by AC, DC, RF and MW sources and the corresponding discharges are named according to the source. The value of the pressure and applied voltage lead many kinds of discharges, such as glow and arc discharges. For all cases there is a threshold for the value of the voltage, which is called as breakdown voltage, and after this value is achieved the gas allows electric current flow. In order to create this an outside radiation source is used to initiate and keep the discharge in some cases. This kind of process is called non-self-sustaining discharge.

Glow discharge is one of the widely used discharge types. It is applied in sputtering processes, spectroscopy and fluorescent lights. The name comes from the glowing gas in many different colors. It is a self-sustaining discharge with a cold cathode and the tube can be filled with a specific gas such as H_2, N_2, Ar or Ne. Mainly it has three layers: (1) The anode layer, (2) the positive column and (3) the cathode layer. The anode layer, where the electrons are dominant, is placed between anode and the positive column. The positive column is relatively neutral part consisting of weakly ionized non-equilibrium plasma. This part is not essential in the process and actually it may disappear at relatively small inter-electrode gap. The cathode layer, where ion concentration is dominating over electrons, is the most essential part in the process. In this layer the voltage drop called cathode fall is higher than the other parts. Theoretically the glow discharge is modeled in different ways. In this work, the fluid model based

on the diffusion-drift theory is employed.

1.3 Modeling

In studying discharge plasmas or gas discharges there are two main approaches available. The first one is the experimental point of view forming the basis for theoretical understanding. The second one is the theoretical approach, which is basically numerical modeling of the processes and their results. In the models the analytical solutions are not available. Therefore numerical approach is an obligatory way to choose.

The governing equations used in this work consist of continuity equations for the electron and positive ion densities coupled to the Poisson equation, called fluid model. The equations constitute a system of nonlinear second-order partial differential equations with appropriate boundary conditions. In applied mathematics, they are also called convection-diffusion-reaction equations. The diffusion and convection terms may depend on magnitude of the local electric field. As a result, the equations become highly non-linear. Additionally, in the numerical cases the fact that convective flux dominates over the diffusive flux, makes the problem numerically harder.

In numerical point of view the differential equation is solved at certain points in the computation domain called grid points. When the number of points approaches infinity; the discrete equations, which are solved numerically, approaches the main governing differential equations. In this work, finite difference method, where the discrete equations are derived by the control volume method, is employed. Moreover, in order to resolve the nonlinearity, the iterative procedure is developed.

CHAPTER 2

GAS DISCHARGE

The term gas discharge refers to initiate and maintain the flow of the electrical current through a specific gas. The molecules or atoms in gas state are electrically neutral and they have low conductivity. As a result, unless the voltage applied is high or the other parameters such as pressure and the ionization threshold of the gas particles are not appropriate, the gas does not allow the significant amount of electrical current. As some value of the applied voltage is achieved either by using or not using an external source the particles are ionized and the existence of electrons is obtained. This certain value of the applied voltage at which gas becomes conductor is called breakdown voltage which depends on the gas type.

The basic experiment equipment used in gas discharge physics, over 150 years, is a cylindrical tube shown in (Figure 2.1) with different sizes, though its shape may be altered for some purposes. The tube may contain specific gas in desired pressure and two electrodes inserted at the ends connected to a closed circuit with a resistor and power supply. The voltage over the tube is so called applied voltage. The resistor, pressure and voltage is altered to observe types of gas discharge. The current for the process can possibly be DC or AC whereas sometimes the tube is filled with electromagnetic field without an external current. For the latter case the particles are excited by absorbing electromagnetic energy. Moreover, other setups are available for specific experiments. In most general setup used in laser applications for glow discharge two parallel plates are positioned and the gas flows between them parallel to the surface of the plates to create lasing medium [1] [3].

For several tens of volts of applied voltage, extremely low current, at the order 10^{-15} A, can be observed with sensitive instruments in which ionization caused by cosmic rays or natural radioactivity. In the process, the charges are pulled by the electric field leading electric

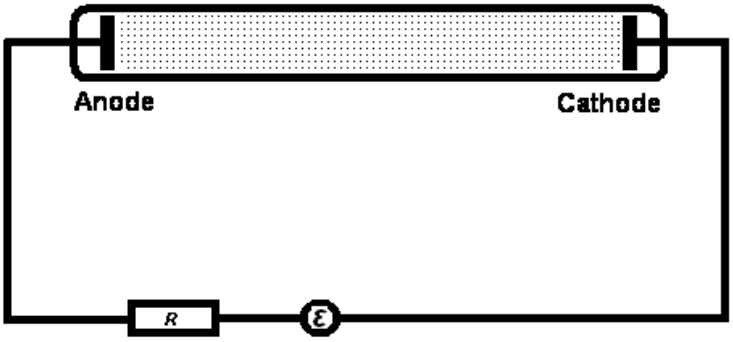

Figure 2.1: Typical gas discharge tube in the circuit. ϵ represents the power supply and R represents the external resistor.

current. For some cases an X-ray or radioactive source is used to initiate the discharge and a current, at the order of 10^{-6} A, is observed without any kind of glow. A raise in the applied voltage increases the current at first, but when all the charges are pulled to the electrodes via the electromagnetic force before the recombination, the current limited by ionization rate seizes to grow. As the voltage raised further on the order of several hundred volts, the bright column shows up itself indicating that the breakdown voltage is achieved. In the breakdown process the small amount of electrons are created naturally or via intentional injection and ionize other particles with the energy gained by the electric field resulting production of more electrons. These less energetic particles gain kinetic energy by the same way and when they reach atomic ionization threshold they start the ionize too. As a result, lots of electrons form a flow and interact with other particles and by the excitations of the gas atoms by these electrons, the light emission is observed. The process takes place in 10^{-9} to several seconds [1].

2.1 Classification

Depending on the physical properties, the discharges can be classified in many different ways. One type of classification is made whether it maintains itself or not. The discharges maintain

themselves without any kind of external source are called self-sustaining, and that can not called non-self-sustaining. Other classification is based on pressure of the process; mainly high pressure and low pressure ones. Another one is based on whether electrodes are used or not. Whether DC current is used or not defines another classification. The last classification depends on the temperature of the the plasma of the discharge. Thermal or quasi equilibrium discharges are relatively hot and non-thermal ones are colder.

2.2 Different Types

High external resistor value results in small current in the circuit, on the order of 10^{-4}-10^{-1} A, the applied voltage values around 10^{2}-10^{3} V and leads to the glow discharge phenomena. The discharge is self-sustaining one with electron emission at the cathode takes place via ion collision to the cathode, called cold cathode. This type of discharge mainly has three parts composed of cathode layer, positive column and the anode layer. Except the layers near the electrodes, the glow discharge is electrically neutral with ions and electrons which makes it basically a kind of plasma. The fact that the plasma itself is luminous gives the process its name. The glow discharge plasma is weakly ionized with 10^{-8}-10^{-6} fraction of ionized atom values. Furthermore, the plasma is non-equilibrium in two respects. Firstly, the temperature of gas including both ions and electrons is much higher than the ambient temperature $T = 300$ K. As a result the system loose heat. Secondly, degree of ionization is magnitudes of lower than the thermodynamic equilibrium value, leading to non-equilibrium. This type of discharge can be divided into four class: (1) Townsend dark discharge, (2) Subnormal glow discharge (3) Normal glow discharge and (4) Abnormal glow discharge [3].

Decreasing the external resistor value leads passage from glow to arc discharge with higher current $I \approx 1 - 10^{5}$ A. This type is DC, self-sustainable and thermal discharge which is basically composed of same parts with the previous type. The basic difference between them, except the current and pressure values, is that the last one has relatively low cathode fall. This is basically caused by the different mechanism of the electron emission of the cathode. In the glow discharge process the cathode emissions are caused by the positive ion impacts with cold cathode. However in the arc discharge the high value of the current heat the cathode and the thermionic emission process yields greater electron current from the cathode. As a result, the electron number density is higher in cathode layer than the density in the previous

one leaving the cathode fall lower in arc discharge. Additionally, this type takes place in low applied voltage values, 20-30 V for short arcs, and in the appropriate conditions as low as several volts. For this type, the great amount of energy taken from the current yields the vaporization at the cathode. It is also observed that in glow discharge the emission spectrum shows the spectrum of the gas inside the tube whereas in arc discharge the emission spectrum also shows the metal cathode. Moreover, in some cases the plasma at the positive column can be in equilibrium. Arc discharge has a wide application in the fields of illumination and metallurgy.

Other type of discharge is the spark discharge that may exist with different values of parameters. Usually, in the laboratory, they occur at ten to hundreds of kV with relatively small inter-electrode distance. Common giant example in the nature to this type is the lightning, where the clouds and ground serve as electrodes. The discharge is transient process where the voltage difference in the gap results in rapid growth of plasma channel between the electrodes and as a result, the spark jumps are observed in the tube like lightning. These jumps zigzag or branch out and disappear very fast. Additionally, the sudden pressure change and resulting shock wave in the plasma channel leads to a sound similar to the thunder. In the process, the spark jump leads the drop in the applied voltage and it vanishes, after the voltage increases again another pulse of spark is observed. If the power supply is capable of creating high voltages spark discharge forms a cathode spot and it turns to be a dark discharge. The process can not be explained by Townsend theory as the others do and the initiation process for this discharge differs than the others by its complexity.

When the uniform field in the spark discharge is replaced by non-uniform one the corona discharge occurs. This one takes place at atmospheric pressure. As a result, it can be observed around the lightning rods and high-voltage transmission conductors. The famous example is St. Elmo's fire. The process has relatively weak luminosity than the others and it takes place locally where the electric field is strong.

Other kind is inductively coupled radio-frequency discharge which is widely used in the laser applications. This one is similar to the glow discharge except the radio-frequency voltage and the pressure parameters. Moreover, Microwave and optical discharges are among the different types [3].

CHAPTER 3

GLOW DISCHARGE

Glow discharge takes its name from the luminous weakly ionized non-equilibrium plasma in the process. Formally, it is self-sustaining, non-thermal DC discharge with a cold cathode, having the secondary electron emission caused by the ion impacts. The physical parameter ranges are shown in (Table 3.1). Compared to other discharges this type occurs at relatively low pressure and current. The most distinctive feature is the high density of the ions near the cathode leading a very high value of cathode fall at values 100 -500 V. Part of this type is so called cathode layer which forms the basic and the most important structure to create the glow discharge. Without this layer the process never takes place. The thickness of this layer is inversely proportional to the pressure or the density of the gas. Structure of this type of discharge mainly forms a weakly ionized middle part after the cathode layer. This layer is named positive column and it does not have even minor role in the process. In some cases where the inter-electrode distance and pressure are low, this layer is never formed though the process takes place. The most amazing property of this layer is the type of plasma it holds. Because of its state the glow discharge is widely used in many areas such as sputtering, spectroscopy etc. Additionally, it allows the study of the plasma medium. The structure ends with a negatively dominant layer called anode layer because the electrons pulled to the anode via the electric field. The layers of a typical DC driven glow discharge in the tube is shown in (Figure 3.3).

Conventional setup of the glow discharge is shown in (Figure 2.1) and it is the mostly used configuration. Other setups are used in different applications, such as film deposition and electron bombardment processes. The magnetron glow discharge setup is widely used in plasma assisted sputtering and deposition, in which magnetic field is used for plasma confine-

Table 3.1: Characteristic parameters of a DC glow discharge in a tube [3].

Discharge tube radius	0.3 – 3.0 cm
Discharge tube length	5 – 100 cm
Gas pressure	0.03 – 30 torr
Applied voltage	100 – 1000 V
Current	10^{-4} – 10^{-1} A
Electron density in positive column	10^{9} – $10^{11} cm^{-3}$

ment. Hollow cathode glow discharge configurations are used in electron bombardment with plasma source. Additionally, the glow discharge plasma is applied in many gas lasers as active medium. In this process, two parallel plates are accompanied and the gas flows between them, though flow does not affect the discharge process in any way. The electrodes may be placed in the plates or on the flow direction. Detailed explanation of the setups are available in [3].

The breakdown process, as many of the discharge modes, is explained by Townsend mechanism, which basically leads the process as a result of the electron avalanche. This process takes place in 0.01 to 100 μs, and the mechanism explains pattern of light emission in this mode of discharge showing itself as luminous and dark layers with a name ascribed each. The light emission is caused by the excitation of the atoms or ions in the process. This whole structure of the glow discharge depends mostly on the electron mean free path, which is inversely proportional to the pressure, leading the light emission pattern lengths and the layers of the discharge inversely proportional to the pressure. The positive column in the process may be composed of periodically placed striations in the light emission pattern. In low pressure and inter-electrode distance this column disappears and only more luminous part called negative glow stays. This glow is responsible for the name of the discharge mode. Additionally, the colors of the light depends on the gas in the tube. Each gas shows different set of colors reflecting its spectrum [1] [3].

One of the most amazing property of the discharge is the current density through the electrodes does not change when the current is increased up to some point, resulted by the minimum power principle. Further raise in the current will lead the discharge evolve and different types of glow discharge occur. Moreover, when the electrodes are rotated axially the whole structure of the discharge rotates with the electrodes leading an axially symmetry [1].

3.0.1 Breakdown Process

The breakdown process is very complicated activity which transforms the non-conductive gas into a conductor, a kind of plasma, starting with electron avalanche. The process in different discharge types are explained by Townsend mechanism discovered by J. S. E. Townsend, student of J. J. Thomson in the beginning of 19. century, though spark and corona discharges can not be explained by this mechanism and streamer or spark mechanism has to be employed to do so.

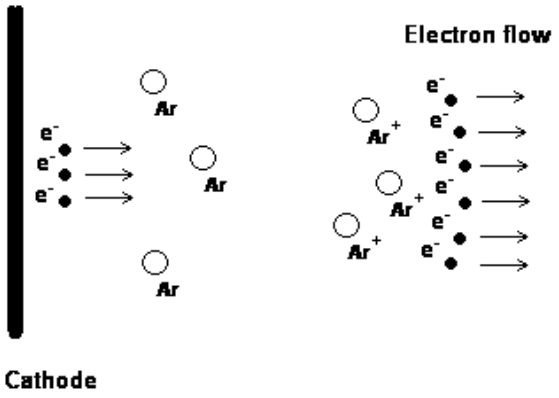

Figure 3.1: The electron avalanche or multiplication process. The initial electrons, emitted by the cathode, get accelerated by the electric field and ionize the atoms. The process creates electrons and ions. These new electrons accelerates by the same mechanism and creates more ions and electrons.

Considering a gas in the tube with an applied potential V and inter-electrode gap h creating uniform electric field $E = V/h$, the initial current value is very low resulted by the effect of the field. Electrons gaining energy by the field starts to ionize the atoms and free electrons leading the electron avalanche. The avalanche evolves in time with the drift of electrons towards to the anode and the uniform field starts to deform. This ionization process continues in the self-sustaining discharge and forms the source of the governing equations.

The ionization process is explained by the Townsend ionization coefficient α rather than an ionization rate coefficient. The coefficient gives the electron production per unit length along the electric field. Simply the coefficient depends on ionization rate coefficient $k_i(E/n_0)$ where

E is the electric field and n_0 is the gas density, and can be expressed as [3]

$$\alpha = \frac{\nu_i}{\nu_d} = \frac{1}{\mu_e}\frac{k_i}{E/n_0} \tag{3.1}$$

where ν_d is electron drift frequency, ν_i is the ionization frequency and μ_e is the electron mobility. Since, the mobility depends on pressure, it is convenient to use α as similarity parameter α/P which depends on the reduced electric field E/P exponentially. This relation can be given as

$$\frac{\alpha}{P} = Aexp(-\frac{B}{E/P}) \tag{3.2}$$

which is conventional and semi-empirical, proposed by Townsend initially. The parameters A and B are empirical values and depends on the gas. According to the mechanism each electron produced near the cathode creates $exp(\alpha h) - 1$ positive ions where h is the inter-electrode distance. In this mechanism, negative ions and electron-ion recombination are negligible. These ions attracted to the cathode collide with it, resulting secondary emitted electrons. In the emission process, secondary emission coefficient γ describing the probability of electron emission of ion impact plays important role. This coefficient depends on the gas, electric field and cathode material. As a result the total electron current at the cathode can be given as

$$I = I_0 + \gamma I[exp(\alpha h) - 1] \tag{3.3}$$

where I_0 is the initial current. Since in the breakdown process the ion current is negligible, the total current can be derived as [3]

$$I = \frac{I_0 exp(\alpha h)}{1 - \gamma[exp(\alpha h) - 1]}, \tag{3.4}$$

the Townsend formula. As the electric field grows to sufficient value the denominator in (Equation 3.4) vanishes and non-self-sustaining discharge turns into self-sustained one, where the breakdown occurs.

3.1 Current Voltage Characteristics

When the breakdown potential is achieved the self-sustaining glow discharge is ignited. Such a current-voltage characteristics of a DC driven glow discharge with the breakdown potential V_t is shown in the (Figure 3.2).

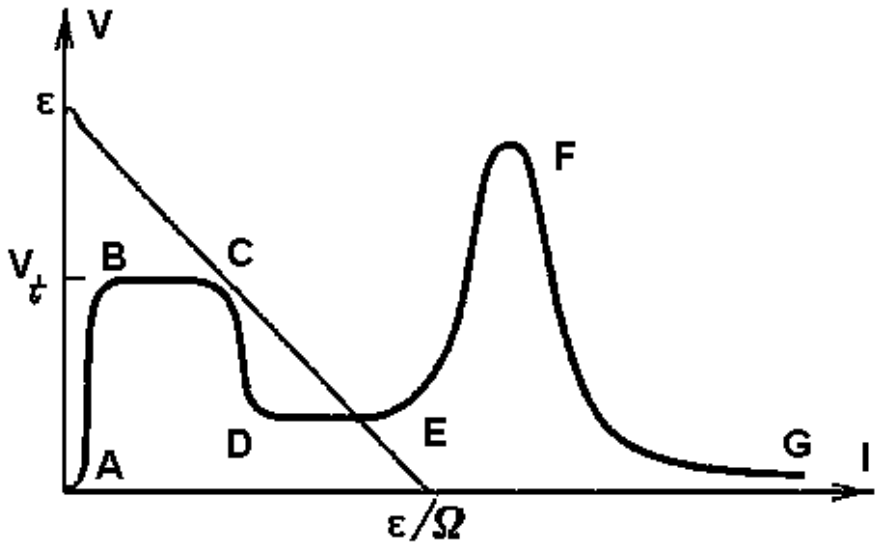

Figure 3.2: Current voltage characteristics of a DC driven glow discharge and the load line [1]. (A) non-self-sustaining discharge, (B-C) Townsend dark discharge, (C-D) subnormal glow discharge, (D-E) normal glow discharge, (E-F) abnormal glow discharge, (F-G)arc discharge initiation and the arc discharge.

The circuit also have an ohmic resistance Ω to arrange the current beside the discharge gap. The Ohm's law for the circuit can be given as

$$\varepsilon = V + \Omega I \tag{3.5}$$

where I is the total current, V is the applied voltage and ε is the power supply voltage. This relation is also called load line, and corresponding straight line is shown in (Figure 3.2). Intersection of the line with the curve gives the actual current in the glow discharge.

Amazingly, further increase in the current yields invariant current density in the normal glow discharge. In the process, area on the cathode where the electrons are emitted plays important role. This area is called cathode spot. As the current increases it expands and results constant current density. The process is explained by the minimum power principle of the Engel-Steenback theory. The power dissipated in the cathode layer is given by [1]

$$P_C = S \int_0^d jE\, dz = S\, jV_C(j) = IV_C(j) \tag{3.6}$$

where d is the cathode layer thickness, $z = 0$ corresponds to the cathode, j is the current density. If the area S enlarges keeping the total current constant, the power released in the cathode

layer is minimum, since $V_C(j)$ is minimum at the given normal current density. Additionally, this minimum power principle also explains the striations in the positive column.

The initial A-B interval represents a non-self-sustaining discharge in (Figure 3.2). After the breakdown is achieved, the current is still low because the ion and electron densities are not sufficient and the uniform electric field is perturbed little. This type is known as Townsend dark or simply dark discharge. The voltage necessary to keep the process is the breakdown voltage. It is shown between B-C in (Figure 3.2). The most distinctive characteristics is the low current about 10^{-10}-10^{-5} A and the plasma density. Raising the power supply potential or lowering the Ω, the dark discharge disappears and transition to the glow discharge is ignited with appearance of subnormal glow discharge. In the process, the ion density and plasma density raise and electric field is disturbed by

$$\nabla \cdot \mathbf{E} = \frac{1}{\varepsilon_0} e(n_i - n_e), \tag{3.7}$$

Maxwell equation for the electric field, where n_i and n_e represent the ion and electron densities respectively. The field is lowered near the anode and the cathode as a result of the process. Additionally, the applied potential is reduced with the current as shown in interval C-D. The current value of this mode is about 10^{-5} to 10^{-4}. In this glow discharge regime, the cathode spot expands to a large value about the cathode layer thickness yielding more electron loss than the normal glow discharge. As a result, the applied potential to keep the process is higher. Further increase in ε or decrease in Ω leads the normal glow discharge, represented as interval D-E in (Figure 3.2). This regime is the actual glow discharge discussed and explained in this work. Increasing the current leads no difference in the current density up to some value, as explained above. Later on, the cathode spot covers entire cathode and has no place to enlarge the current density starts to increase and abnormal glow discharge regime is reached, represented by E-F in the (Figure 3.2). In this regime $V(I)$ is growing and limited by cathode overheating. After, cathode is sufficiently heated and the current value is increased up to 1 A the transition from glow to arc discharge occurs. Another regime of glow discharge other than the normal exists at the low pressure and inter-electrode gap. This mode is called obstructed glow discharge and because of the short gap, electron multiplication is not sufficient to sustain the process and the applied potential should be increased [1].

3.2 The Layers

The layers of normal, DC driven glow discharge , responsible for the pattern of light emission is shown in the (Figure 3.3). In general these layers form dark and bright columns, with different intensities and colors, representing the spectrum of the gas. These structures were first observed by M Faraday in 1830 and appear on a wide range of parameter values [2].

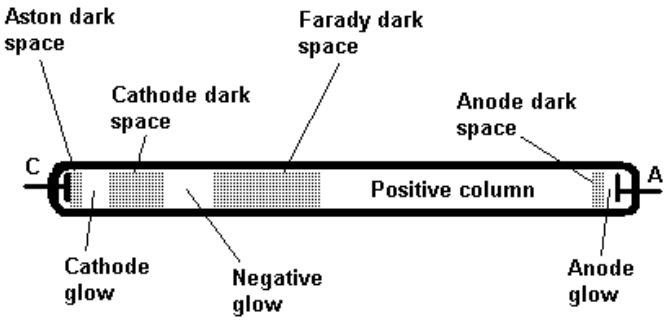

Figure 3.3: Layers of a typical DC driven glow discharge [1] [3].

The region near the cathode is Aston dark space, where the electrons emitted from the cathode are accelerated. This part is dominated by the positive ions and resulting high electric field. Additionally, it forms the first part of the cathode layer. Next to this region the electrons gained enough energy and excite the atoms, resulting light emission, called cathode glow. The ion density is relatively higher than the one at the Aston dark space. The electrons having more energy yields the low value of the probability of collision and cathode dark space is formed near the cathode glow. The cathode glow has the highest ion density in general. In the following region, negative glow, the brightest of the all layers, appears. The excitation of the atoms by the slow electrons is responsible for the light emission and the ionization is resulted by the energetic electrons. The region is brightest near the cathode dark space and gradually looses brightness toward the anode. The charge density decreases in the following layers because of the recombination and diffusion toward the walls, and leaves a dark layer. This region where the electric field is lower is called Faraday dark space. Next to this, the

positive column stands. This structure is weakly-ionized and the electric field is only strong enough to keep the ionization at the cathode end. It shows long, uniform glow except the form of standing or moving striations and ionization waves. The striations are produced by the perturbation in the electron density. The positive column disappears at low pressure and inter-electrode distance. Passing the positive column the brighter anode glow layer shows itself, and may not be always present in the discharge. The final regime is the anode dark space where the negative charges are dominant, standing between the anode and the anode glow. The electric field in this region is higher than the one in the positive column [1] [3].

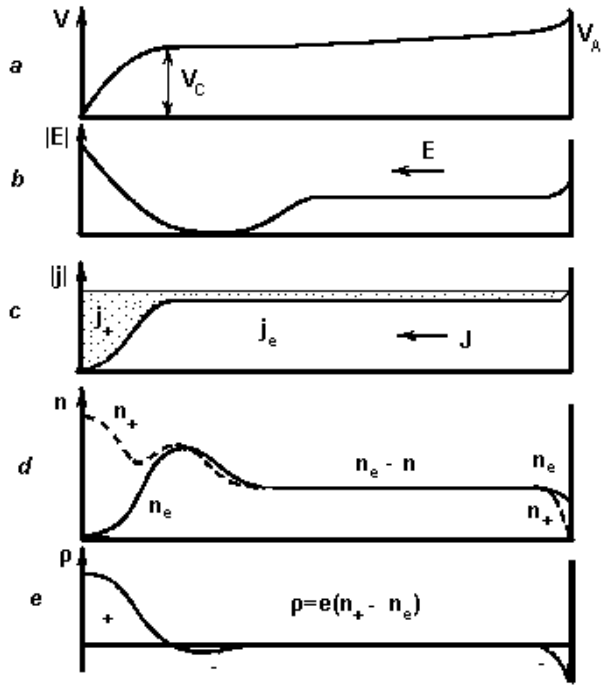

Figure 3.4: The characteristics of a typical glow discharge along the tube [1]. (a) Potential, (b) electric field, (c) ion and electron current densities, (d) ion and electron number densities, (e) net charge.

In the discharge process, the cathode layer plays the most important role of accelerating the electrons to sustain the discharge. Additionally it generates sufficient current to the plasma flux in the positive column. Though the positive column is interesting in the applications of the glow discharge, it does not play any significant role in the discharge. Moreover, though the anode layer is necessary for the process, it is not as important as cathode layer.

3.2.1 Cathode Layer

The applied voltage to the tube is not sufficient to form a discharge because of the uniformity of the electric field. It is known that the sufficient amount of non-uniformity of the electric field is created to keep sustaining discharge by the high positive charge dominance near the cathode. This gives the cathode layer its importance in the process.

To describe the cathode layer, a theory is developed by Engel and Steenback in 1934. The theory matches the experimental data and it is very important in the process. Developing the theory, they firstly realized that the electric field at the end of the cathode layer $E(z = d)$ is lower than the the one at the cathode $E(z = 0) = E_C$. Also they discovered that the ion flux from the positive column is negligible because of the low ion mobility and assumed $E(z = d) = 0$. Then the potential drop can be approximated as

$$V_C = \int_0^d E\, dz. \tag{3.8}$$

They reached the conclusion [3]

$$E(z) = E_C(1 - z/d), \quad 0 < z < d \tag{3.9}$$

$$E(z) = 0, \qquad\qquad z > d. \tag{3.10}$$

They found cathode fall relations similar to Paschen curves describing the breakdown of the discharge [3]

$$V_C = \frac{B(Pd)}{C + ln(Pd)}, \frac{E_C}{P} = \frac{B}{C + ln(Pd)} \tag{3.11}$$

where $C = lnA - lnln(1/\gamma + 1)$, A and B are the parameters of ionization coefficient (Equation 3.2), P is the pressure and d is the cathode layer length. Conventionally, the distance in the glow discharge is given by the scale $distance \times pressure$ because of the pressure dependence. Hence conventionally speaking the cathode layer length can be given as Pd.

Although it seems that the glow discharge can occur in many current densities, the process prefers a certain value which correspond to the minimum of cathode fall V_C (Equation 3.11). The glow discharge taking place with this parameter is referred normal glow discharge and the parameters are called normal current density, normal voltage etc.

3.2.2 Positive Column

Positive column is the part where the big amount of the power is released, which leads to the wide usage in the laser applications and chemical engineering. Though it is long homogeneous part of the process, the glow discharges are possible without this column. It is composed of the weakly-ionized non-equilibrium plasma, where the electron and ion densities are almost equal and these properties are independent of the ones in the anode and cathode layers. These properties depend on the applied potential and the ionization processes in the layer. Basically in this layer, the loss of charged particles due to the recombination must be balanced with the ionization, which leads to the behavior of the electric field. Generally speaking, this electric field in the structure is almost constant and yields voltage difference linear with slight slope.

3.2.3 Anode Layer

The anode layer is the regime between the anode and the positive column, where the electron density is dominant. This behavior is basically caused by the absence of the ion emission at the anode. The electron generation in this regime is low compared to the cathode layer. As a result the potential drop is relatively small.

3.3 Qualitative Explanation of the Process

The qualitative explanation was firstly proposed by Townsend, and it only describes the process without numerical values, since the process occurs in a complicated many-particle system with many interactions.

The electrons ejected from the cathode with energy about 1 eV which is not sufficient for the excitation. As a result Aston dark space is formed. The electrons gain energy passing through the this region via the electric field and they reach the sufficient energies to excite the atoms and the cathode glow shows itself. The cathode glow may have up to three columns and each column corresponds to the energy levels of the gas atoms. The first column near the Aston dark space has the least energetic excitation energy and grows linearly with the levels since more away from the cathode more energy electrons gain. The colors of the columns

reflect the spectrum of the gas. Passing this layer electrons gain more energy and as a result the cross-section decreases significantly as shown in [1] [3]. Hence, the cathode dark space appears. In this region ionization is dominant and as a result the ion density increases and the electron multiplication is very high. After the process, newly generated electrons have lower energies and moving toward the anode forms the negative glow. The cathode end of the negative glow shows the highest intensity. It decreases later on because the electric field decreases and the electrons are not accelerated sufficiently at the end of the cathode layer, somewhere in the negative glow. Electrons dissipate energy and can not gain. As a result, the Faraday dark space stands after the negative glow. In this layer the electric field increases up to special value of the positive column and electrons gain more energy and the excite the neutral atoms in the positive column. Moreover, the existence of energetic electrons which interact little and come from cathode allows the ionization. Further away from the positive column, the electrons do not have sufficient energy for excitation resulting the formation of anode dark space. The anode pulls the electrons and repels the ions making negative charge density dominant which yields the higher electric field. The electrons get accelerated again and forms the anode glow.

3.4 Governing Equations

To explain a plasma there are three theories used in different assumptions. The first one is the Kinetic theory which covers almost whole process of the plasma. The distribution function in this theory lives in 6 dimensional phase space $\varphi = \varphi(x, y, z, v_x, v_y, v_z, t)$ where the first three set is the space coordinates and the next three are the corresponding velocities with the last one as time coordinate. The second one is the fluid theory which can be divided into less detailed one fluid (only one fluid type), the more complex and detailed two-fluid theory. This theory is less complex than the kinetic theory. Moreover, theory uses the Maxwellian distribution function in coordinate space, which leads the theory valid for this type of distribution. When one uses the Maxwellian distribution in kinetic equations with appropriate assumptions one reaches the governing equation of fluid theory. Basic form of the fluid theory considers the plasma as a one self interacting fluid. The more detailed form is the two fluid equation where the plasma is considered as negatively charged and positively charge fluids by interacting themselves and each other. Finally, the least complex theory can be given as Magnetohydrodynamic equations

which explains single, finite pressure, electrically conducting plasma as fluid [4].

3.4.1 Two-Fluid Theory

The theory does not try the hard task of finding trajectories of the particles. In the plasma particles are affected by the electromagnetic field and they create field too. Though, plasma and fluid have different characteristics of interactions, the plasma is governed by similar equations. The strong electromagnetic interactions in the plasma take place between the charged particles. However, in the fluid only local effect of electrical and magnetic moments are responsible for the interactions. The plasma is assumed as a fluid and the motion of the fluid elements are considered instead of individual fluid particles. Though, there is one fluid description mentioned in [6] [7], it is more applicable to use the two-fluid description. This description takes the electrons and ions as two different fluids interacting with each other and neutral atoms. It should be emphasized that the electrons and ions interact even if the collisions are absent via the electromagnetic field [4].

The two fluid equations of plasma for electrons are

$$\frac{\partial n_e}{\partial t} + \nabla \cdot n_e \mathbf{u}_e = S \tag{3.12}$$

$$m_e n_e \frac{d\mathbf{u_e}}{dt} = -en_e(\mathbf{E} + \mathbf{u}_e \times \mathbf{B}) - \nabla P_e + \mathbf{F}_{ei} \tag{3.13}$$

and for ions

$$\frac{\partial n_i}{\partial t} + \nabla \cdot n_i \mathbf{u}_i = S \tag{3.14}$$

$$m_i n_i \frac{d\mathbf{u_i}}{dt} = en_i(\mathbf{E} + \mathbf{u}_i \times \mathbf{B}) - \nabla P_i + \mathbf{F}_{ie}, \tag{3.15}$$

supplemented by the equations of state and appropriate boundary conditions, where n_e, n_i are electron and ion densities respectively, $\mathbf{u}$ is the velocity, $\mathbf{F}$ is frictional force (effect of elastic collisions), S is the source term, m is the mass of the particle and e is the charge. The electric $\mathbf{E}$ and magnetic $\mathbf{B}$ fields are explained by the Maxwell equations

$$\varepsilon_0 \nabla \cdot \mathbf{E} = \rho \tag{3.16}$$

$$\nabla \times \mathbf{E} = -\frac{\partial \mathbf{B}}{\partial t} \tag{3.17}$$

$$\nabla \cdot \mathbf{B} = 0 \tag{3.18}$$

$$\nabla \times \mathbf{B} = \mu_0(\mathbf{j} + \varepsilon_0 \frac{\partial \mathbf{E}}{\partial t}) \tag{3.19}$$

where **j** is current and **u** is the velocity of the charged particle.

The basic equation for electron fluid in the plasma, which is momentum exchange or Newton's law can be written with a general force **F**

$$mn_e \frac{d\mathbf{u}_e}{dt} = \mathbf{F} \tag{3.20}$$

Basically, the force must have electromagnetic part, Lorentz force, which can be written as

$$\mathbf{F} = -e(\mathbf{E} + \mathbf{u}_e \times \mathbf{B}). \tag{3.21}$$

However, in this work we do not consider the magnetic field effects. In the cases where the magnetic field is applied to the gas discharge medium this effect can be considered. As a result electromagnetic part of the force is given as

$$\mathbf{F}_E = -e\mathbf{E}. \tag{3.22}$$

Considering thermal motions of the the particles, one should take account of the pressure too. At a point in plasma where the pressure is higher than the points around , one expects that the diffusion of the pressure results in a force at that point. This force will be in the opposite direction of the increasing pressure and depends on how high the pressure raises. Hence, the force of the pressure must be in the form

$$\mathbf{F}_P = -\nabla P_e. \tag{3.23}$$

The detailed derivation of the force is explained in [4] [7]. One should note that, though we assumed the plasma fluid is isotropic, it is also possible that the momentum in one direction can be transferred in other direction. In such case, instead of scalar pressure, one takes a tensor describing the pressure called stress tensor.

In the plasma there are two kinds of collision types. The first one is the elastic collision which does not change the internal structures of the colliding particles and only the momentum is transferred. Other type is the inelastic collisions in which the internal structures of the colliding particles change. This type of collisions are responsible for the ionization, excitation and recombination of the particles [5] [6]. As a result the momentum changes with elastic collisions and one should take into account of this in the above equations as

$$\mathbf{F}_{ei} = -mn_e\nu_{ef}(\mathbf{u}_e - \mathbf{u}_f). \tag{3.24}$$

where $\mathbf{u}_f$ represents the velocity of other fluid the electron fluid interacts, and ν_{ef} is the collision frequency. Note that this force can be taken as frictional forces. Hence total change of the momentum can be written as

$$mn_e \frac{d\mathbf{u}}{dt} = -e\mathbf{E} - \nabla P_e - mn_e \nu_{ef}(\mathbf{u}_e - \mathbf{u}_f). \tag{3.25}$$

Moreover, in the left hand side of the equation time derivative is taken in the position of the fluid element and it is not useful. Instead of this one should take the derivative in a fixed position. To do so, one takes a fixed reference frame in which the fluid flow inside then the velocity depends on time and the position of the fluid element with respect to this reference frame. With the application of the change of coordinates time derivative is written as

$$\frac{d\mathbf{u}(x,t)}{dt} = \frac{\partial \mathbf{u}}{\partial t} + \frac{\partial \mathbf{u}}{\partial x}\frac{dx}{dt} = \frac{\partial \mathbf{u}}{\partial t} + \frac{\partial \mathbf{u}}{\partial x} u_x \tag{3.26}$$

or in more appropriate form

$$\frac{d\mathbf{u}(x,t)}{dt} = \frac{\partial \mathbf{u}}{\partial t} + (\mathbf{u} \cdot \nabla)\mathbf{u} \tag{3.27}$$

which is called convective derivative. Moreover the frame can be taken as moving with acceleration with taking corresponding inertial forces as explained in [4] [7]. As a result, the equation in the glow discharge for electrons is

$$m_e n_e \frac{\partial \mathbf{u_e}}{\partial t} + (\mathbf{u_e} \cdot \nabla)\mathbf{u_e} = q\mathbf{E} - \nabla P_e - m_e n_e \nu_{en}(\mathbf{u_e} - \mathbf{u}_n) - m_e n_e \nu_{ei}(\mathbf{u_e} - \mathbf{u}_i) \tag{3.28}$$

The similar process yields the equation for the ions as

$$m_i n_i \frac{\partial \mathbf{u_i}}{\partial t} + (\mathbf{u_i} \cdot \nabla)\mathbf{u_i} = q\mathbf{E} - \nabla P_i - m_i n_i \nu_{in}(\mathbf{u_i} - \mathbf{u}_n) - m_i n_i \nu_{ie}(\mathbf{u_i} - \mathbf{u}_e) \tag{3.29}$$

where e represents the electron, i ions and n neutral atoms. These equations are so similar to the Navier-Stokes equation except the electrical force terms. The viscosity in a fluid is given as elastic collisions in these equations.

In the steady state the velocities does not change with time but the position hence partial time derivative of the velocity vanishes and if the collision frequency is large or the velocity is sufficiently small then vanishing convective derivative is good approximation [4].

Since the electron velocity is much higher than the ion and neutral atom velocities and putting pressure term $P_e = kT_e n_e$ the equation of electron fluid yields

$$n_e \mathbf{u_e} = -\frac{kT_e}{m_e \nu_e}\nabla n_e - \frac{e}{m_e \nu_e} n_e \mathbf{E} \tag{3.30}$$

where electron collision frequency is approximated as the sum of the collision frequencies given. Moreover, the equation can be put in more suitable form as

$$n_e \mathbf{u_e} = -D_e \nabla n_e - \mu_e \mathbf{E} n_e \tag{3.31}$$

where

$$D_e = \frac{kT_e}{m_e \nu_e} \tag{3.32}$$

$$\mu_e = \frac{e}{m_e \nu_e} \tag{3.33}$$

diffusion and mobility of the electron fluid, which are related by Einstein relation [4]. Assuming that

$$\nu_{ie} m_i n_i (\mathbf{u}_i - \mathbf{u}_e) = -\nu_{ei} m_e n_e (\mathbf{u}_e - \mathbf{u}_i) \tag{3.34}$$

$$\mathbf{u}_n = 0 \tag{3.35}$$

$$m_e \nu_e << m_i \nu_{in} \tag{3.36}$$

ion equation leads the similar relation

$$n_i \mathbf{u_i} = -D_i \nabla n_i + \mu_i \mathbf{E} n_i \tag{3.37}$$

with ion diffusion and mobility

$$D_e = \frac{kT_i}{m_i \nu_{in}} \tag{3.38}$$

$$\mu_e = \frac{e}{m_i \nu_{in}}. \tag{3.39}$$

The velocities of the electron and ion can be taken as the fluxes or the currents in the plasma in the form

$$\mathbf{\Gamma}_e = n_e \mathbf{u_e}, \quad \mathbf{\Gamma}_i = n_i \mathbf{u_i}. \tag{3.40}$$

One more physical idea in the two fluid theory is the conservation of matter. The relation can be derived from divergence theorem as

$$\frac{\partial n}{\partial t} + \nabla \cdot \mathbf{\Gamma} = S \tag{3.41}$$

where the term in the right hand side represents the source or sink for the charge. The creation or annihilation of the charges is related to the ionization coefficient and recombination

coefficient. Since, the main reason of the ionization is the electron current and the recombination, the source is related to the ion and electron densities with these parameters. Hence, the equations can be written as [19]

$$\frac{\partial n_e}{\partial t} + \nabla \cdot \mathbf{\Gamma}_e = \bar{\alpha} \left| \mathbf{\Gamma}_e \right| - \bar{\beta} n_e n_i \tag{3.42}$$

$$\frac{\partial n_i}{\partial t} + \nabla \cdot \mathbf{\Gamma}_i = \bar{\alpha} \left| \mathbf{\Gamma}_e \right| - \bar{\beta} n_e n_i, \tag{3.43}$$

with the (Equation 3.7) and the electric potential

$$-\nabla^2 V = \frac{e}{\epsilon_0}(n_i - n_e). \tag{3.44}$$

3.4.2 Coefficients

The coefficients for electrons and ions are taken from [21]-[32]. For the ionization term a generalization of Townsend coefficient is taken as

$$\bar{\alpha}(E/n)/n = \begin{cases} -2.748 \times 10^{-18} \sqrt{E/n} + 4.04 \times 10^{-19} E/n & \\ -7.40 \times 10^{-23} (E/n)^2 & \text{for } E/n > 67.8 \text{ Td}, \\ 1.406 \times 10^{-23} (E/n)^3 & \text{for } E/n \leq 67.8 \text{ Td} \end{cases} \tag{3.45}$$

and another approximation is

$$\begin{aligned} \bar{\alpha}(E/n) \quad = \quad & n 1.1 \times 10^{-18} e^{-72n/E} \\ & + 5.5 \times 10^{-17} e^{-187n/E} \\ & + 3.2 \times 10^{-16} e^{-700n/E} \\ & - 1.5 \times 10^{-16} e^{-10000n/E} \end{aligned} \tag{3.46}$$

where the gas density is taken as $n = 3.54 \times 10^{16} m^{-3}$ corresponding 1 *torr* pressure at 273 K. The other coefficients are

$$\mu_i(E) = \frac{4.411 \times 10^{19}}{(1 + (7.721 \times 10^{-3} E/n)^{1.4})^{0.33} n} \quad \frac{cm^2}{sV}, \qquad D_i = 0.025 \mu_i \quad \frac{cm^2}{storr} \tag{3.47}$$

$$\mu_e = 3 \times 10^5 \quad \frac{cm^2}{sVtorr}, \qquad D_e = 3 \times 10^5 \quad \frac{cm^2}{storr} \tag{3.48}$$

$$\gamma = 0.07, \qquad \beta = 1.085 \times 10^{-9}. \tag{3.49}$$

where mobility and diffusion of ions are related by Einstein relation and with another expressions of ion mobility and ion diffusion are

$$\mu_i(E) = \begin{cases} \frac{(1-2.22\times10^{-3}E/p)}{p} & E/p \leq 60 \quad \frac{V}{cmtorr} \\ \frac{8.25\times10^{13}}{p\sqrt{E/p}}(1-\frac{86.52}{(E/p)^{3/2}}) & \text{for } E/p > 60 \quad \frac{V}{cmtorr} \end{cases} \tag{3.50}$$

$$D_i = 2\times10^2 \quad \frac{cm^2}{storr}. \tag{3.51}$$

For the tube, we take the cylindrical coordinates and use the axial symmetry where h corresponding to cathode and reference frame is fixed at anode.

$$U = 350 \quad V \qquad h = 5 \quad cm \tag{3.52}$$

$$R = 1.5 \quad cm \tag{3.53}$$

3.4.3 Boundary Conditions

Absence of ions and absence of electron emission are given at the anode $z = 0$, as boundary conditions. At the cathode $z = h$, the conditions represent the secondary emission of electrons and absence of ion emission. Moreover, the value of the applied potential is represented by these conditions.

$$n_i(z=0,r) = 0, \qquad \frac{\partial n_e(z=0,r)}{\partial z} = 0 \tag{3.54}$$

$$n_e(z=h,r) = \frac{\gamma\mu_i}{\mu_e} n_i(z=h,r), \qquad \frac{\partial n_i(z=h,r)}{\partial z} = 0 \tag{3.55}$$

$$V(z=0,r) = 0, \qquad V(z=h,r) = -U, \tag{3.56}$$

where γ is the secondary emission coefficient. The conditions at the side walls represent the Neumann conditions.

$$\frac{\partial n_i(z,r=R)}{\partial r} = 0, \quad \frac{\partial n_e(z,r=R)}{\partial r} = 0 \tag{3.57}$$

$$\frac{\partial n_i(z,r=0)}{\partial r} = 0, \quad \frac{\partial n_e(z,r=0)}{\partial r} = 0 \tag{3.58}$$

$$\frac{\partial V(z,r=0)}{\partial r} = 0, \qquad \frac{\partial V(z,r=R)}{\partial r} = 0. \tag{3.59}$$

3.5 Model Equations in Dimensionless form

Though, it is possible to analyze the equations numerically as given form, the dimensionless equations allows the control over the values. Hence, (Equations 3.42-3.44) should be turned

into dimensionless form with appropriate parameters. The parameters and the continuity equations can be put into this form with

$$\tau = \frac{t}{t_0}, \quad \mathbf{x} = \frac{\mathbf{r}}{r_0}, \tag{3.60}$$

$$\sigma = \frac{n_e}{n_0}, \quad \rho = \frac{n_i}{n_0}, \tag{3.61}$$

$$\mathcal{E} = \frac{\mathbf{E}}{E_0}, \quad \phi = \frac{V}{R_0 E_0} \tag{3.62}$$

$$\mathcal{D}_{i,e} = \frac{D_{i,e}}{\mu_e E_0 R_0}, \quad \mu = \frac{\mu_i}{\mu_e} \tag{3.63}$$

$$\alpha = \frac{\bar{\alpha}}{\alpha_0}, \quad \beta = \frac{\bar{\beta}\epsilon_0}{e\mu_e} \tag{3.64}$$

as in [19], where $\mathcal{E}$ is dimensionless electric field vector. Then they take the form.

$$\frac{\partial \sigma}{\partial \tau} - \nabla \cdot (\mathcal{D}_e \nabla \sigma + \mathcal{E}\sigma) = \alpha \left| \mathcal{D}_e \nabla \sigma + \mathcal{E}\sigma \right| - \beta \sigma \rho \tag{3.65}$$

$$\frac{\partial \rho}{\partial \tau} - \nabla \cdot (\mathcal{D}_i \nabla \rho - \mu \mathcal{E}\rho) = \alpha \left| \mathcal{D}_i \nabla \sigma + \mathcal{E}\sigma \right| - \beta \sigma \rho \tag{3.66}$$

$$-\nabla^2 \phi = (\rho - \sigma) \tag{3.67}$$

$$\mathcal{E} = -\nabla \phi \tag{3.68}$$

with the arrangements

$$r_0 = \frac{1}{\alpha_0}, \quad t_0 \frac{r_0}{\mu_e E_0} \tag{3.69}$$

$$n_0 = \frac{\epsilon_0 \alpha_0 E_0}{e}. \tag{3.70}$$

CHAPTER 4

NUMERICAL APPROACH AND RESULTS

The improvements in computer technology and the Numerical Analysis allow us to solve the problems where the analytical result is not available. These situations are very common and show themselves as nonlinear equations. By this way, one can predict the convenience of the model of a physical situation or predict the outcome of certain processes. The most astonishing numerical applications are recently developed numerical relativity, the applications in plasma physics and fluid dynamics.

The approach employed in the numerical computation is the Finite Difference method based on the approximation of the differential equation with discrete equations via control volume or Taylor series approach. The fact that the computation domain is flat in our calculations lead us to ignore the Finite Element method based on the variational formulation or Galerkin method. Moreover, the profile assumption of the dependent variable is sufficient in the method [10][13].

Basically, in numerical approach one divides the computation domain in grid points as shown in (Figure 4.1) and approximates the differential equation at these points. By this way the continuous solution and the differential equation are transformed into discrete solution and algebraic equations. As the grid spacing goes to zero, the discrete solution and the algebraic equation goes to continuous solution and the differential equation. The methods employed in this work does not only include applied mathematics but the physical laws are also considered. The discretization method (control volume formulation) is solely based on the conservation principles (conservation of particles in this work) in every grid cell of the computation domain.

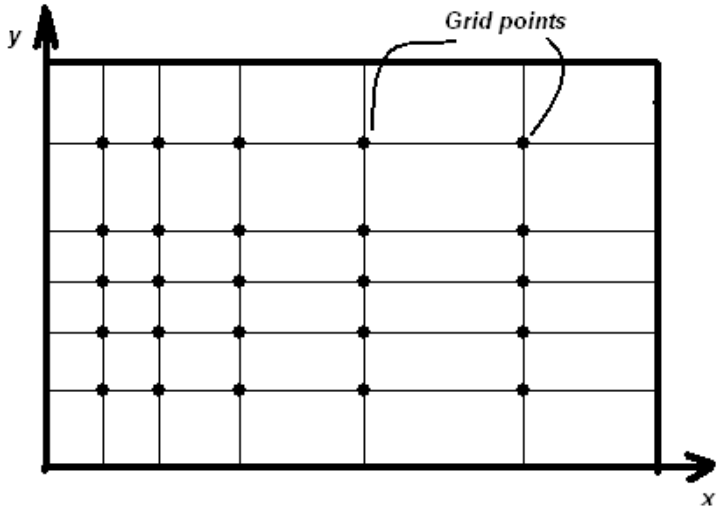

Figure 4.1: The grid points over the computation domain.

In the process of computation, firstly one-dimensional counterpart of axially symmetric, stationary partial differential equation in z direction is to be analyzed numerically and then the partial differential equations given in (Chapter 4) are to be solved. In some texts they are also called time-dependent advection-diffusion-reaction equations [17].

4.1 Grid and Discretization

First procedure in the numerical solution is the choice of the grid arrangement. The arrangement may affect the numerical convergence and accuracy of the solutions. In some cases the arrangement yields perturbations from the exact solution. Basically, one may choose these points spaced uniformly over the computation domain and have so-called uniform grid distribution (constant spacing). The choice of number of grids affects the computation time and accuracy in the process. As a result one should avoid increasing or decreasing number of grids too much. The appropriate number of grids can be chosen according to how much the approximate solution of the numerical process changes with different arrangements. How-

ever, it is more convenient to increase the number of grid points where the solution changes more. This type of grid distribution is called non-uniform grid distribution.

After the appropriate choice of the grid, the discretization is focused on. Basically, discrete or finite difference equation is the simple algebraic equation derived from the differential equation, and solution of this gives the numerical result. The choice of the discretization method simply defines how the solution behaves between the grid points. By this way, the behavior of the solution is controlled over the computation sub-domains. Though, for all different type of the discretization, the resulting equations converges to the corresponding differential equation for a large number of grids and the choice of the method only defines the profile attributed to the exact solution. This profile forms the basic difference between the Finite Difference Method and the Finite Element method. These discretization formulations are also classified by the derivation of the method, beside the profile of the dependent variable between the grid points.

The discrete equations can be derived in many ways. The mostly used method is the Taylor series formulation, which is given in many introductory books. In this formulation the derivatives are approximated by using truncated Taylor series. For three numbered grid points, as shown in (Figure 4.2) such that $\Delta z = z_2 - z_1 = z_3 - z_2$, truncated Taylor series around the second are

$$f_1 \approx f_2 - \Delta z \left[\frac{df}{dz}\right]_2 + \frac{1}{2}(\Delta z)^2 \left[\frac{d^2 f}{dz^2}\right]_2 \tag{4.1}$$

$$f_3 \approx f_2 + \Delta z \left[\frac{df}{dz}\right]_2 + \frac{1}{2}(\Delta z)^2 \left[\frac{d^2 f}{dz^2}\right]_2 . \tag{4.2}$$

Subtracting and summing them gives the approximations for the derivatives [13]

$$\left[\frac{df}{dz}\right]_2 \approx \frac{f_3 - f_1}{2\Delta z} + O(\Delta z^2) \tag{4.3}$$

$$\left[\frac{d^2 f}{dz^2}\right]_2 \approx \frac{f_1 - 2f_2 + f_3}{\Delta z^2} + O(\Delta z^3). \tag{4.4}$$

The method is appropriate if the function dependence is polynomial. Moreover, also higher order derivatives can be approximated. However, they lead more computation load because of the several grid points [14] and higher order differential equations can be transformed into the form of lower order set of differential equations. The first derivative of the function at higher order approximations such as $O(\Delta z^n)$, $n > 2$ can be derived with the same method. For

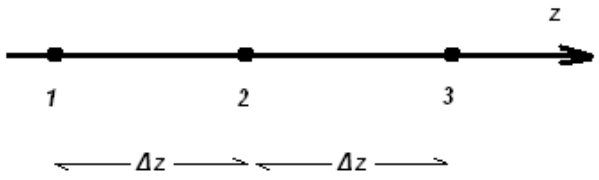

Figure 4.2: Basic grid points over one dimensional computation domain [13].

example so called Euler methods yield higher order approximations. Nonetheless, this leads more computation. Instead, smaller grid spacing can arrange more accurate approximations

The derived approximation is the so called centered difference scheme. In addition to this forward or backward difference schemes can be derived in the formulation. These approximations differ in the order of the remainder terms. For instance, backward difference scheme for the first derivative can be written as [10]

$$\left[\frac{df}{dz}\right]_2 = \frac{f_2 - f_1}{\Delta z}. \tag{4.5}$$

Different discretization formulations can be applied at specific conditions [13]. The formulation employed in the process is the control volume approach. In this technique, the grid points are surrounded by non-overlapping control volume cells, as shown in (Figure 4.3). In each cell, the conservation of the certain quantity is achieved. This physical property of the formulation lets it perfect candidate to use in the computation. In our case the conserved quantity is particle conservation. The control volume cell distribution used in this work is so called cell centered grids, in which the cells hold the grid points at their centers and creating a ghost points outside the computation domain leading ghost cells [14] [17]. The ghost points are preferred to be lifted in this work by the arrangement of the control volume cells.

4.1.1 Θ-Method

The system of the form $\frac{\partial u}{\partial t} + Lu = S$ is solved explicitly if the solution is to be found as

$$\frac{u^{k+1} - u^k}{\Delta t} + L^k u^k = S^k, \tag{4.6}$$

where k defines the iteration. Such a numerical approach is called explicit method. However, in some cases the explicit solution is not useful and implicit methods must be used or they are preferable. Additionally, mixed form of the implicit and explicit approaches are available such as the Crank-Nicholson method in which the expression

$$\frac{u^{k+1} - u^k}{\Delta t} + L^k(\frac{1}{2}u^{k+1} + \frac{1}{2}u^k) = S^k \tag{4.7}$$

is used to solve the next iteration [12]. Most general form of this approach,employed in this work, is the θ-method given as

$$\frac{u^{k+1} - u^k}{\Delta t} + L^k(\theta u^{k+1} + (1-\theta)u^k) = S^k, \tag{4.8}$$

where $0 \leq \theta \leq 1$, is used.

4.1.2 Time Step and Iteration

Because the parameters depend on the function to be investigated in nonlinear problems, the solution needs initial guess. Basically, the initial guess function is one of the reasons affecting the computation time and convergence criteria. Iterative solution of the nonlinear problems is processed in this work and other methods can be applied depending on the problem [10]. In the process of iteration, firstly the initial guess is approximated and the parameters are defined according to it [11]. After the computation, the new solution is used to define the parameters. This process continues until the differential equation is satisfied up to a tolerance value. Moreover, the tolerance value can be taken as the difference between the solutions before the iteration and after it. This value, called error of convergence, can be used as a overall rude tool to see the convergence. For a general equation of the form $\frac{\partial u}{\partial t} + Lu = S$, the iterative computation can be represented as

$$\frac{u^{k+1} - u^k}{\tau} + L^k u^{k+1} = S^k \tag{4.9}$$

where k represents the iteration, τ is the time parameter and u^{k+1} is to be calculated.

The glow discharge relaxes to a steady state after a time, leading stationary model of the fluid theory. As a result, either stationary equations are to be solved or the time dependent equations are solved till the system converges stationary state. Calculations showed that the first one is unstable, hence the later is used in the computation. In this model the approximation of the time dependence can be achieved by the similar methods used in the spatial derivatives with some differences. The approximation for the time derivative is chosen to be

$$\frac{\partial u}{\partial t} \approx \frac{u^{k+1} - u^k}{\Delta t}. \tag{4.10}$$

where k represents the iteration number, and the value of the function at u^{k+1} is to be computed.

In the first trial of the computation, the vanishing time derivative is assumed. Afterwards, the time dependency was put into account by a proper choice of time step Δt. The convergence of the numerical method strongly depends on this value. Generally, the value should be taken according to the spatial grid, diffusion and convection parameters. The conditions for the convergence are generally described by the von Neumann conditions for linear problems. However, they are unavailable for nonlinear problems. Moreover, if time step is taken so low, then the convergence becomes slow and computation time increases, if it is taken so high some of the convergence criteria may not be achieved. Available time step criteria for uniform grid with θ-method is [16]

$$\Delta t \leq \frac{1}{1-\theta} \Bigg/ \left(\frac{|C_r|}{\Delta r} + \frac{|C_z|}{\Delta z} + \frac{2D}{\Delta r^2} + \frac{2D}{\Delta z^2} \right). \tag{4.11}$$

To apply in non-uniform grid and dependent parameters the expression

$$\Delta t \leq k \min \left[\frac{1}{1-\theta} \Bigg/ \left(\frac{|C_r|}{\Delta r} + \frac{|C_z|}{\Delta z} + \frac{2D}{\Delta r^2} + \frac{2D}{\Delta z^2} \right) \right] \tag{4.12}$$

is approximated with $0 < k < 1$.

4.1.3 Boundary Conditions and Error

The boundary conditions are put by hand into the solution. For Dirichlet boundary conditions the values are put to satisfy them. For Neumann boundary conditions, a ghost point can be created outside the computation domain. However, for the conditions of the form

$$\frac{df(0)}{dz} = a \tag{4.13}$$

the value at the boundary is chosen to be satisfy

$$\frac{f(z(2)) - f(z(1))}{z(2) - z(1)} = a. \tag{4.14}$$

There are mainly three types of criteria need to be satisfied to obtain appropriate result. These are consistency, convergence and stability [10] [14] [17]. In the methods the errors of the computation at each iteration may show whether the convergence conditions are satisfied or not. Three main types of errors are used in the computation [17] [18]. Additionally, another overall convergence error is used to observe the overall convergence and steady state solutions. For a discrete equation of the form $Lu = S$ the errors are

$$\|e\|_1 = \sum_{n,m=1}^{N,M} E_{nm}\Delta z_n \Delta r_m \tag{4.15}$$

$$\|e\|_2 = \sqrt{\sum_{n,m=1}^{N,M} E_{nm}^2 \Delta z_n \Delta r_m} \tag{4.16}$$

$$\|e\|_\infty = \max[E_{nm}] \tag{4.17}$$

$$\tag{4.18}$$

where

$$E_{nm} = |(Lu - S)_{nm}|, \tag{4.19}$$

and n and m defines the grid numbers. The overall error employed is

$$Error = \frac{\max\left|u^{k+1} - u^k\right|}{\max\left|u^k\right|} \tag{4.20}$$

where k defines the iteration number. One should note that, in other cases of control volume approach it may be better to use the differential equations rather than the discretization equations to define the error terms.

4.2 One Dimensional Model

Though, the uniform grid was employed at first, non-uniform grid with closer grid points at the cathode layer is chosen, according to the result. The grid points are closer near the cathode and they recede as they get closer to the anode. This is done by some exponential function of special form with some arrangement parameters. The expression for the grid function along the tube is

$$x_n = a + (b - a)\frac{e^{\nu(n-1)/(N-1)} - 1}{e^\nu - 1} \quad n = 1, 2, \ldots N \tag{4.21}$$

where $a = 0$ is the origin, $b = h$ is the end of the computation domain, N is the total number of grid points, n is the number representing the grid point and $\nu = -5$ is the parameter to arrange the grid point distribution. The convergence is efficient with $N = 60$, total number of grid points.

The corresponding one dimensional equations (Chapter 4) are set in the form

$$\frac{\partial \sigma}{\partial \tau} - \frac{\partial}{\partial z}\left(\mathcal{D}_e \frac{\partial \sigma}{\partial z}\right) - \frac{\partial}{\partial z}(\mathcal{E}\sigma) = \alpha \left|\mathcal{D}_e \frac{\partial \sigma}{\partial z} + \mathcal{E}\sigma\right| - \beta\sigma\rho \tag{4.22}$$

$$\frac{\partial \rho}{\partial \tau} - \frac{\partial}{\partial z}\left(\mathcal{D}_i \frac{\partial \rho}{\partial z}\right) + \frac{\partial}{\partial z}(\mu\mathcal{E}\rho) = \alpha \left|\mathcal{D}_e \frac{\partial \sigma}{\partial z} + \mathcal{E}\sigma\right| - \beta\sigma\rho \tag{4.23}$$

$$-\frac{\partial^2 \phi}{\partial z^2} = \rho - \sigma \tag{4.24}$$

$$\mathcal{E} = -\frac{\partial \phi}{\partial z} \tag{4.25}$$

with the boundary conditions

$$\rho(z = 0) = 0, \quad \partial_z \sigma(z = 0) = 0 \tag{4.26}$$

$$\sigma(z = h) = \gamma\mu\rho(z = h), \quad \partial_z \rho = 0 \tag{4.27}$$

$$V(z = 0) = 0, \qquad V(z = h) = -U. \tag{4.28}$$

where τ is time parameter, ρ ion density, σ electron density, $\mathcal{E}$ electric field, and ϕ electric potential.

The equations can be reduced in the form of one-dimensional advection diffusion equation as

$$\frac{\partial \eta}{\partial t} - \frac{\partial}{\partial z}\left(D \frac{\partial \eta}{\partial z}\right) + \frac{\partial}{\partial z}(C\eta) = S \tag{4.29}$$

where D stands for diffusion, C is for convection or advection and S is for source term. For one dimensional computation domain shown in (Figure 4.3), the equation is to be integrated over the control volume cell in the application of the control volume approach. This will lead us the discrete equation.

Integration with the time step application yields

$$\frac{\eta - \bar{\eta}}{\Delta t}\Delta z - \left(D \frac{\partial \eta}{\partial z}\right)_{\omega}^{e} + (C\eta)_{\omega}^{e} = \int_{\omega}^{e} S \, dz = < S > \Delta z \tag{4.30}$$

with the assumption that over the infinitesimally small cell the values ar constant, where Δz is the distance between the control volume walls, Δt is the time step, $< S >$ is the mean value

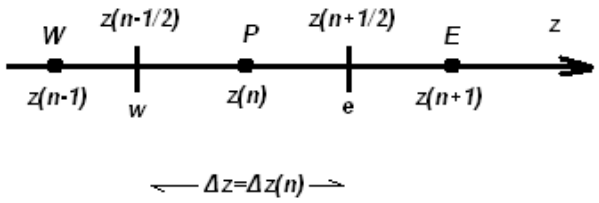

Figure 4.3: The grid points over one dimensional computation domain. Main points are given by the integers in the parentheses and by the capital letters [13].

over the cell, $\bar{\eta}$ is the result of previous iteration. All the dicretization process takes place in the middle of the cell, at point P. The time step employed with θ-method takes the form

$$\Delta t \leq k \min\left[\frac{1}{1-\theta}\Big/\left(\frac{C}{\Delta z}+\frac{2D}{\Delta z^2}\right)\right]. \tag{4.31}$$

The terms with diffusion can be approximated by the Taylor series formulation results

$$\left(D\frac{\partial \eta}{\partial z}\right)_{\omega} = (D)_{\omega}\,\frac{\eta_P-\eta_W}{z_P-z_W} \tag{4.32}$$

$$\left(D\frac{\partial \eta}{\partial z}\right)_{e} = (D)_{e}\,\frac{\eta_E-\eta_P}{z_E-z_P} \tag{4.33}$$

where we can approximate the diffusion terms at the control volumes by interpolation. For the convection terms, another profile called upwind scheme is to be used, instead of the interpolation. The scheme chooses the convection term as a determining parameter in the process, and the principle of conservation is satisfied. Between two main grid points the direction of the convection chooses the main grid point to be employed and can be written in the form

$$(C\eta)_{\omega} = \eta_W[[C_{\omega},0]] - \eta_P[[-C_{\omega},0]] \tag{4.34}$$

$$(C\eta)_{e} = \eta_P[[C_{e},0]] - \eta_E[[-C_{e},0]] \tag{4.35}$$

where $[[a,b]]$ stands for the maximum value in the parentheses.

With the application of θ method this leads to one dimensional discretization equations of the form

$$+B_1\eta_1 - C_1\eta_2 = F_1 \tag{4.36}$$

$$-A_n\eta_{n-1} + B_n\eta_n - C_n\eta_{n+1} = F_n \quad n = 2, 3, \ldots N-1 \tag{4.37}$$

$$-A_N\eta_{N-1} + B_N\eta_N = F_N \tag{4.38}$$

where N is the number of grids, n defines the grid cell or grid point and

$$A_n = \theta\Delta t\left(\frac{D_{n-1/2}}{z_n - z_{n-1}} + [[C_{n-1/2}, 0]]\right) \tag{4.39}$$

$$B_n = \Delta z_n + \theta\Delta t\left(\frac{D_{n+1/2}}{z_{n+1} - z_n} + \frac{D_{n-1/2}}{z_n - z_{n-1}} + [[C_{n+1/2}, 0]] + [[-C_{n-1/2}, 0]]\right) \tag{4.40}$$

$$C_n = \theta\Delta t\left(\frac{D_{n+1/2}}{z_{n+1} - z_n} + [[-C_{n+1/2}, 0]]\right) \tag{4.41}$$

$$F_n = S_n\Delta z_n\Delta t + (1-\theta)\frac{A_n}{\theta}\bar{\eta}_{n-1} + (1-\theta)\frac{C_n}{\theta}\bar{\eta}_{n+1} - \left((1-\theta)\frac{B_n - \Delta z_n}{\theta} - \Delta z_n\right)\bar{\eta}_n \tag{4.42}$$

with $n = 2, 3, \ldots N-1$, where $\bar{\eta}$ defines the previous iteration result. The equations at first grid number 1 and the last one N represent the boundary conditions, where the A,B,C and D values are chosen to satisfy the corresponding ones. As can be seen some of the values of A and C are not used. These values are chosen to be zero.

4.2.1 Thomas Algorithm

The one dimensional equations can be put in the matrix form as

$$\begin{pmatrix} B_1 & C_1 & 0 & \ldots & 0 \\ A_2 & B_2 & C_2 & 0 & \vdots \\ 0 & A_3 & \ddots & \ddots & \\ \vdots & 0 & \ddots & \ddots & C_{N-1} \\ 0 & \ldots & 0 & A_N & B_N \end{pmatrix} \begin{pmatrix} \eta_1 \\ \eta_2 \\ \vdots \\ \eta_N \end{pmatrix} = \begin{pmatrix} F_1 \\ F_2 \\ \vdots \\ F_N \end{pmatrix}$$

When the system of algebraic equations of the form

$$L_{N\times N}u_{N\times 1} = F_{N\times 1} \tag{4.43}$$

are to be solved there are many direct and iterative methods. The method employed may yield extra computation load, if not applied appropriately. However, if one has a tridiagonal matrix,

of the given form, L the equation can be solved easily by a direct method called Thomas algorithm. The method uses LU decomposition for this specific form of tridiagonal matrix.

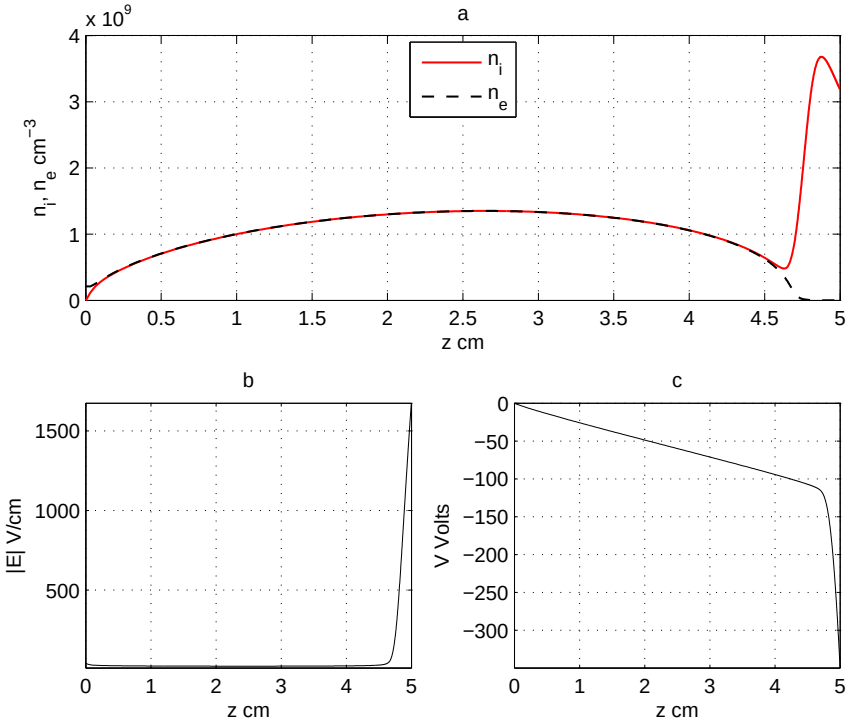

Figure 4.4: One dimensional computational results along the tube at 1 *torr* pressure, 350 V applied voltage and 5 *cm* inter-electrode distance, where $z = 0$ represents the anode and $z = 5$ represents the cathode. (a) The ion and electron densities. (b) The norm of the electric field. and (c) the electric potential.

The Gauss elimination yields the Thomas algorithm

$$B_1 = B'_1 \tag{4.44}$$

$$B'_i = B_i - \frac{A_i}{B'_{i-1}} C_{i-1} \qquad (i = 2, 3, \ldots, N) \tag{4.45}$$

$$b_1 = b'_1 \tag{4.46}$$

$$b'_i = b_i - \frac{A_i}{B'_{i-1}} b'_{i-1} \qquad (i = 2, 3, \ldots, N) \tag{4.47}$$

and the solution is get by the back substitution of the calculated values by the algorithm;

$$u_N = \frac{b'_N}{B'_N} \tag{4.48}$$

$$u_i = \frac{b'_i - C_i u_{i+1}}{B'_i} \qquad (i = N-1, N-2, \ldots, 1). \tag{4.49}$$

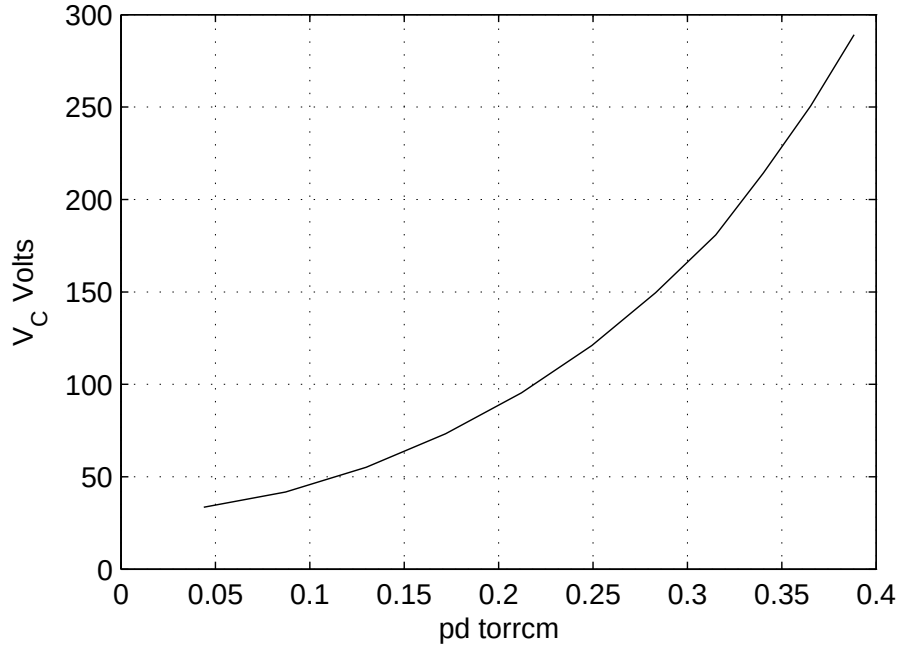

Figure 4.5: Cathode fall V_C, cathode layer length pd graph.

4.2.2 Results

One dimensional computational results, given in (Figure 4.4) are similar to the ones in [1] [19] [20]. As expected high number of ion density is observed in cathode layer with cathode fall at the order of 250 V. The neutral positive column and the anode layer which is dominated by electrons showed themselves along the tube. The relation between the cathode fall and cathode layer length is shown in (Figure 4.5). The result shows similarity with [1] [3] for argon.

Different approximations for ion mobility, ion diffusion, ionization coefficient are analyzed. The approximations for the ionization coefficient, given in (Chapter 4) are

$$\bar{\alpha}(E/n)/n = \begin{cases} -2.748 \times 10^{-18}\sqrt{E/n} + 4.04 \times 10^{-19} E/n & \\ -7.40 \times 10^{-23}(E/n)^2 & \text{for } E/n > 67.8 \text{ Td}, \\ 1.406 \times 10^{-23}(E/n)^3 & \text{for } E/n \leq 67.8 \text{ Td} \end{cases} \tag{4.50}$$

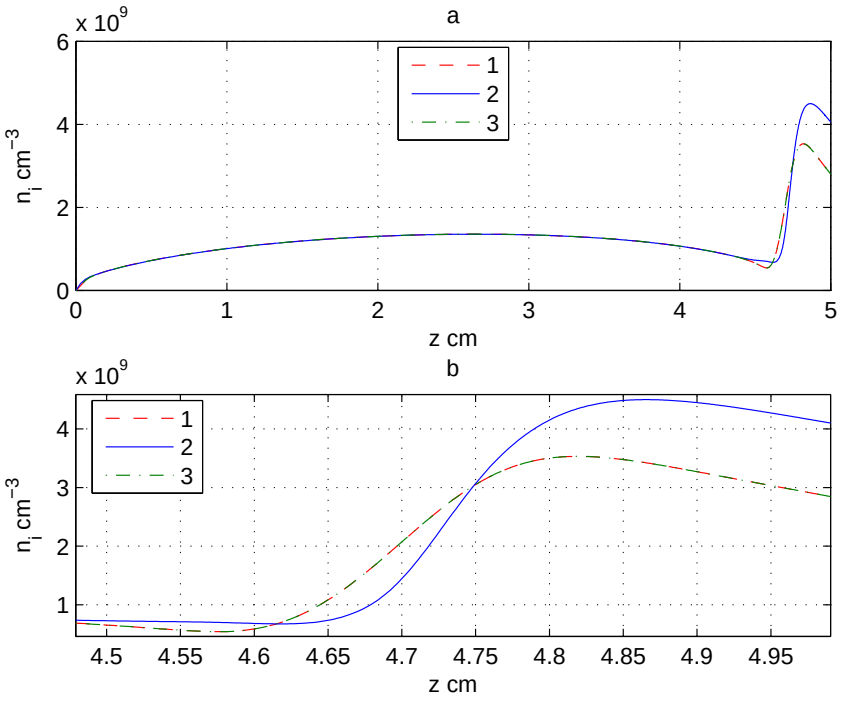

Figure 4.6: The ion number densities along the tube with different coefficients. (a) Overall picture, (b) zoomed to the cathode layer.

$$\begin{aligned}\bar{\alpha}(E/n) &= n1.1\times10^{-18}e^{-72n/E} \\ &\quad + 5.5\times10^{-17}e^{-187n/E} \\ &\quad + 3.2\times10^{-16}e^{-700n/E} \\ &\quad - 1.5\times10^{-16}e^{-10000n/E}. \end{aligned} \tag{4.51}$$

The two given expressions of the ion mobility are

$$\mu_i(E) = \frac{4.411\times10^{19}}{(1+(7.721\times10^{-3}E/n)^{1.4})^{0.33}n} \quad \frac{cm^2}{sV} \tag{4.52}$$

$$\mu_i(E) = \begin{cases} \frac{(1-2.22\times10^{-3}E/p)}{p} & E/p \le 60 \quad \frac{V}{cmtorr} \\ \frac{8.25\times10^{13}}{p\sqrt{E/p}}(1-\frac{86.52}{(E/p)^{3/2}}) & \text{for } E/p > 60 \quad \frac{V}{cmtorr}. \end{cases} \tag{4.53}$$

The two ion diffusion terms are

$$D_i = 0.025\mu_i \quad \frac{cm^2}{storr} \tag{4.54}$$

$$D_i = 2\times10^2 \quad \frac{cm^2}{storr}, \tag{4.55}$$

where (Equation 4.54) represents the Einstein relation. As a result, the choice of ionization coefficient differs significantly especially in the cathode layer, though choice of mobility and diffusion does not yield any difference. Moreover, the exclusion of the recombination coefficient from the source does not change the results significantly. In (Figure 4.6), for (1) (Equations 4.50, 4.52, 4.54) are used. For (2), instead of ionization coefficient (Equation 4.50), the other expression (Equation 4.51) is taken. Additionally, in (3) the coefficients of (1) are used excluding the recombination coefficient.

4.3 Two Dimensional Model

Since large perturbations are not expected in radial direction, the same grid function with one dimensional case (Equation 4.21) is used with different values of ν to create approximately constant grid spacings. For the computation domain total number of grids along the tube $N = 60$ and in the radial direction in cylindrical coordinates $M = 80$ were appropriate. Owing to the physical process shows the axial symmetry, the constancy of the solution with respect to θ direction is assumed.

The equations to be solved in two dimensions are in the form

$$\frac{\partial \sigma}{\partial \tau} - \nabla \cdot (\mathcal{D}_e \nabla \sigma + \mathcal{E}\sigma) = \alpha \left| \mathcal{D}_e \nabla \sigma + \mathcal{E}\sigma \right| - \beta \sigma \rho \tag{4.56}$$

$$\frac{\partial \rho}{\partial \tau} - \nabla \cdot (\mathcal{D}_i \nabla \rho - \mu \mathcal{E}\rho) = \alpha \left| \mathcal{D}_e \nabla \sigma + \mathcal{E}\sigma \right| - \beta \sigma \rho \tag{4.57}$$

$$-\nabla^2 \phi = \rho - \sigma \tag{4.58}$$

$$\mathcal{E} = -\nabla \phi, \tag{4.59}$$

where $\mathcal{E}$ is the dimensionless electric field vector, with the boundary conditions

$$\rho(z = 0, r) = 0, \qquad \frac{\partial \sigma(z = 0, r)}{\partial z} = 0 \tag{4.60}$$

$$\sigma(z = h, r) = \gamma \mu \rho(z = h, r), \qquad \frac{\partial \sigma(z = h, r)}{\partial z} = 0 \tag{4.61}$$

$$\frac{\partial \sigma(z, r = R)}{\partial r} = 0, \quad \frac{\partial \rho(z, r = R)}{\partial r} = 0 \tag{4.62}$$

$$\frac{\partial \sigma(z, r = 0)}{\partial r} = 0, \quad \frac{\partial \rho(z, r = 0)}{\partial r} = 0 \tag{4.63}$$

$$\phi(z = 0, r) = 0, \qquad \phi(z = h, r) = -U \tag{4.64}$$

$$\frac{\partial \phi(z, r = 0)}{\partial r} = 0, \qquad \frac{\partial \phi(z, r = R)}{\partial r} = 0. \tag{4.65}$$

The similar process of control volume approach occurs in two dimensional case. The grid points and the control volume are given in (Figure 4.7). The partial differential equation can be written in a general form as

$$\frac{\partial \eta}{\partial t} - \nabla \cdot (D \nabla \eta) + \nabla \cdot (\mathbf{C}\eta) = S, \tag{4.66}$$

and in the cylindrical coordinates with the axial symmetry it takes the form

$$\frac{\partial \eta}{\partial t} - \frac{1}{r}\frac{\partial}{\partial r}\left(D\frac{\partial \eta}{\partial r}r\right) - \frac{\partial}{\partial z}\left(D\frac{\partial \eta}{\partial z}\right) + \frac{1}{r}\frac{\partial}{\partial r}(\eta r C_r) + \frac{\partial}{\partial z}(\eta C_z) = S. \tag{4.67}$$

where the subscripts in the convection defines the components of the vector $\mathbf{C}= (C_r, C_z)$. For the general equation of the form

$$\frac{\partial u}{\partial t} + Lu = S, \tag{4.68}$$

the integration will be in the form

$$\int_\omega^e \int_s^n \left(\frac{\partial u}{\partial t} + Lu\right) r dr\, dz = \int_\omega^e \int_s^n S\ r dr\, dz. \tag{4.69}$$

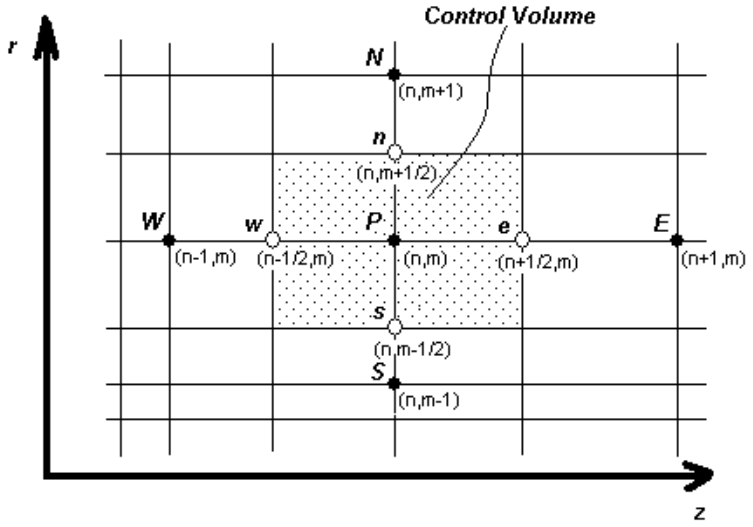

Figure 4.7: The grid points over two dimensional computation domain. The numbers in the parentheses represent the point number. Main points are defined by integers and capital letters. The control volume walls are given by the small letters [13].

With the similar assumptions as in one dimensional case and the application of time step, this will lead us

$$\frac{\eta-\bar{\eta}}{\Delta t}r\Delta r\Delta z-\left(D\frac{\partial\eta}{\partial r}r\right)_s^n\Delta z-\left(D\frac{\partial\eta}{\partial z}\right)_\omega^e r\Delta r+(\eta rC_r)_s^n\Delta z+(\eta C_z)_\omega^e r\Delta r=S\,r\Delta r\Delta z, \tag{4.70}$$

where $\bar{\eta}$ defines the previous iteration.

The diffusion and convection terms are put according to the same method in one dimensional calculation. The diffusion terms are approximated as

$$\left(D\frac{\partial\eta}{\partial r}r\right)_n=(Dr)_n\frac{\eta_N-\eta_P}{r_N-r_P} \tag{4.71}$$

$$\left(D\frac{\partial\eta}{\partial r}r\right)_s=(Dr)_s\frac{\eta_P-\eta_S}{r_P-r_S} \tag{4.72}$$

$$\left(D\frac{\partial\eta}{\partial z}\right)_e=(D)_e\frac{\eta_E-\eta_P}{z_E-z_P} \tag{4.73}$$

$$\left(D\frac{\partial\eta}{\partial z}\right)_\omega=(D)_\omega\frac{\eta_P-\eta_W}{z_P-z_W} \tag{4.74}$$

$$\tag{4.75}$$

and the convection terms with upwind scheme are

$$(C_r\eta r)_n=r_n\left(\eta_P[[(C_r)_n,0]]-\eta_N[[-(C_r)_n,0]]\right) \tag{4.76}$$

$$(C_r\eta r)_s=r_s\left(\eta_S[[(C_r)_s,0]]-\eta_P[[-(C_r)_s,0]]\right) \tag{4.77}$$

$$(C_z\eta)_e=\eta_P[[(C_z)_e,0]]-\eta_E[[-(C_z)_e,0]] \tag{4.78}$$

$$(C_z\eta)_\omega=\eta_W[[(C_z)_\omega,0]]-\eta_P[[-(C_z)_\omega,0]]. \tag{4.79}$$

As a result of the process two dimensional algebraic equations with θ method take the form

$$-A_{nm}\eta_{(n,m+1)}-B_{nm}\eta_{(n+1,m)}+C_{nm}\eta_{(n,m)}-D_{nm}\eta_{(n,m-1)}-E_{nm}\eta_{(n-1,m)}=F_{nm} \tag{4.80}$$

where n and m defines the grid points along the tube and r direction respectively. Taking total grids N and M for the coordinates respectively, $n=2,3,\dots N-1$ and $m=2,3,\dots M-1$ are given. The expressions in the (Equation 4.80) are

$$A_{nm}=\theta\Delta t\left(\frac{D_{(n,m+1/2)}}{r_{m+1}-r_m}\Delta z_n r_{m+1/2}+r_{m+1/2}[[(C_r)_{(n,m+1/2)},0]]\Delta z_n\right) \tag{4.81}$$

$$B_{nm}=\theta\Delta t\left(\frac{D_{(n+1/2,m)}}{z_{n+1}-z_n}\Delta r_m r_m+r_m[[(C_z)_{(n+1/2,m)},0]]\Delta r_m\right) \tag{4.82}$$

$$C_{nm}=r_m\Delta r_m\Delta z_n+\theta\Delta t\left(\frac{D_{(n,m+1/2)}}{r_{m+1}-r_m}r_{m+1/2}\Delta z_n+\frac{D_{(n,m-1/2)}}{r_m-r_{m-1}}r_{m-1/2}\Delta z_n\right) \tag{4.83}$$

$$+\theta\Delta t\left(\frac{D_{(n+1/2,m)}}{z_{n+1}-z_n}r_m\Delta r_m+\frac{D_{(n-1/2,m)}}{z_n-z_{n-1}}r_m\Delta r_m\right)$$
$$+\theta\Delta t\left(r_{m+1/2}[[(C_r)_{(n,m+1/2)},0]]\Delta z_n\right)$$
$$+\theta\Delta t\left(r_{m-1/2}[[-(C_r)_{(n,m-1/2)},0]]\Delta z_n\right)$$
$$+\theta\Delta t\left([[(C_z)_{(n+1/2,m)},0]]r_m\Delta r_m\right)$$
$$+\theta\Delta t\left([[-(C_z)_{(n-1/2,m)},0]]r_m\Delta r_m\right)$$

$$D_{nm}=\theta\Delta t\left(\frac{D_{(n,m-1/2)}}{r_m-r_{m-1}}\Delta z_n r_{m-1/2}+r_{m-1/2}[[(C_r)_{(n,m-1/2)},0]]\Delta z_n\right) \tag{4.84}$$

$$E_{nm}=\theta\Delta t\left(\frac{D_{(n-1/2,m)}}{z_n-z_{n-1}}\Delta r_m r_m+r_m[[(C_z)_{(n-1/2,m)},0]]\Delta r_m\right) \tag{4.85}$$

$$F_{nm}=S_{nm}r_m\Delta r_m\Delta z_n+(1-\theta)\left(\frac{A_{nm}}{\theta}\right)\bar{\eta}_{(n,m+1)}+(1-\theta)\left(\frac{B_{nm}}{\theta}\right)\bar{\eta}_{(n+1,m)} \tag{4.86}$$

$$+(1-\theta)\left(\frac{D_{nm}}{\theta}\right)\bar{\eta}_{(n,m-1)}+(1-\theta)\left(\frac{E_{nm}}{\theta}\right)\bar{\eta}_{(n-1,m)}$$
$$-\left((1-\theta)\frac{B_{nm}-r_m\Delta r_m\Delta z_n}{\theta}-r_m\Delta r_m\Delta z_n\right)\bar{\eta}_{(n,m)}$$

where the diffusion parameter is given partially at the control volumes walls and D_{nm} should not be confused with it. Additionally, the equation is not solved at the boundaries and the values of the function put by hand.

4.3.1 Successive Over Relaxation Method

For two dimensional algebraic equations, one may form the matrix equations and solve them by appropriate direct or iterative methods. In this process, the matrix equation needs to be arranged properly. In this case, it should be noted that the matrix is not tridiagonal. Although, there are Thomas algorithm and other direct methods such as alternating direction implicit method (ADI), in this work Gauss Seidell and successive over relaxation (SOR) iterative methods are used.

Gauss Seidell method initially computes first point[1] using the initial guess and step by step calculates other points. In the process, latest available solutions are used. For the given algebraic equations it can be written as [14]

$$\eta_{(n,m)}=\frac{1}{C_{nm}}\left[F_{nm}+A_{nm}\bar{\eta}_{(n,m+1)}+B_{nm}\bar{\eta}_{(n+1,m)}+D_{nm}\eta_{(n,m-1)}+E_{nm}\eta_{(n-1,m)}\right] \tag{4.87}$$

[1] For this case near the boundary.

$$For \quad n = 2, 3, \ldots, N-1$$

$$For \quad m = 2, 3, \ldots, M-1$$

where $\bar{\eta}$ represents the initial guess or the solution of the previous iteration.

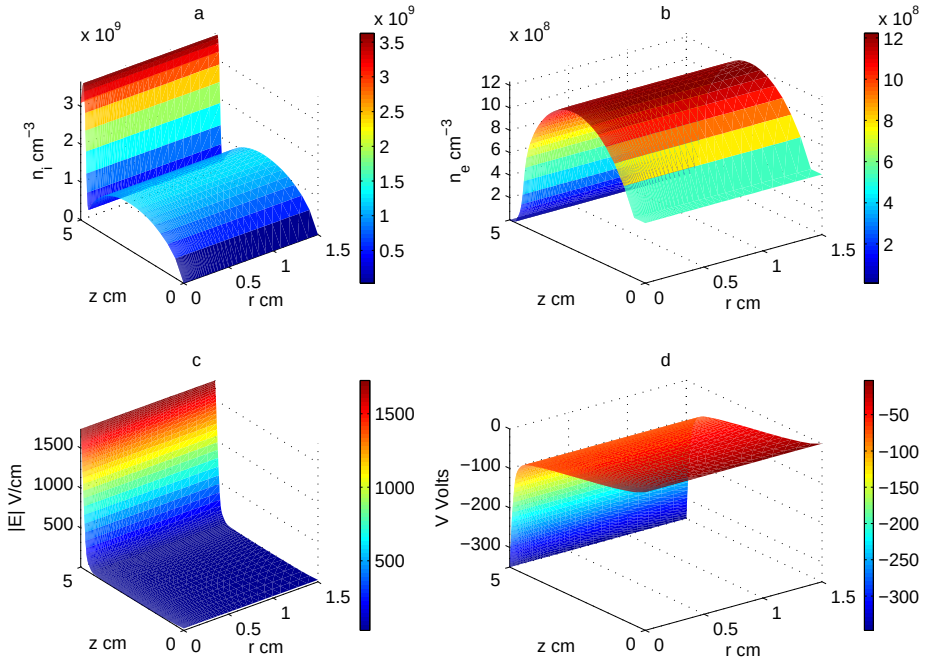

Figure 4.8: Two dimensional computational results at 1 *torr* pressure, 350 V applied voltage and 5 *cm* inter-electrode distance, where $z = 0$ represents the anode and $z = 5$ the cathode. (a) The ion density, (b) the electron number density, (c) the electric field norm, and (d) the electric potential.

Successive over relaxation method is evolved version of Gauss Seidell method. The same expression holds in these methods too and can be written as

$$\eta_{(n,m)}^{k+1/2} = \frac{1}{C_{nm}} \left[F_{nm} + A_{nm}\eta_{(n,m+1)}^{k} + B_{nm}\eta_{(n+1,m)}^{k} + D_{nm}\eta_{(n,m-1)}^{k+1/2} + E_{nm}\eta_{(n-1,m)}^{k+1/2} \right] \tag{4.88}$$

$$\eta_{nm}^{k+1} = \lambda\eta_{nm}^{k+1/2} + (1-\lambda)\eta_{nm}^{k}$$

$$For \quad n = 2, 3, \ldots, N-1$$

$$For \quad m = 2, 3, \ldots, M-1 \quad \lambda > 0$$

where k stands for the iteration number. The expression turns into Gauss Seidell when $\lambda = 1$.

4.3.2 Results

In two dimensional model, the results are shown in (Figure 4.8). The solutions do not differ from the one dimensional case in radial direction, as expected. Moreover, the boundary conditions leading the absence of creation of ions and electrons at the radial boundary of the tube may not be appropriate for the process. More physical and appropriate boundary conditions at the side walls of the tube may yield more appropriate results.

4.4 Convergence

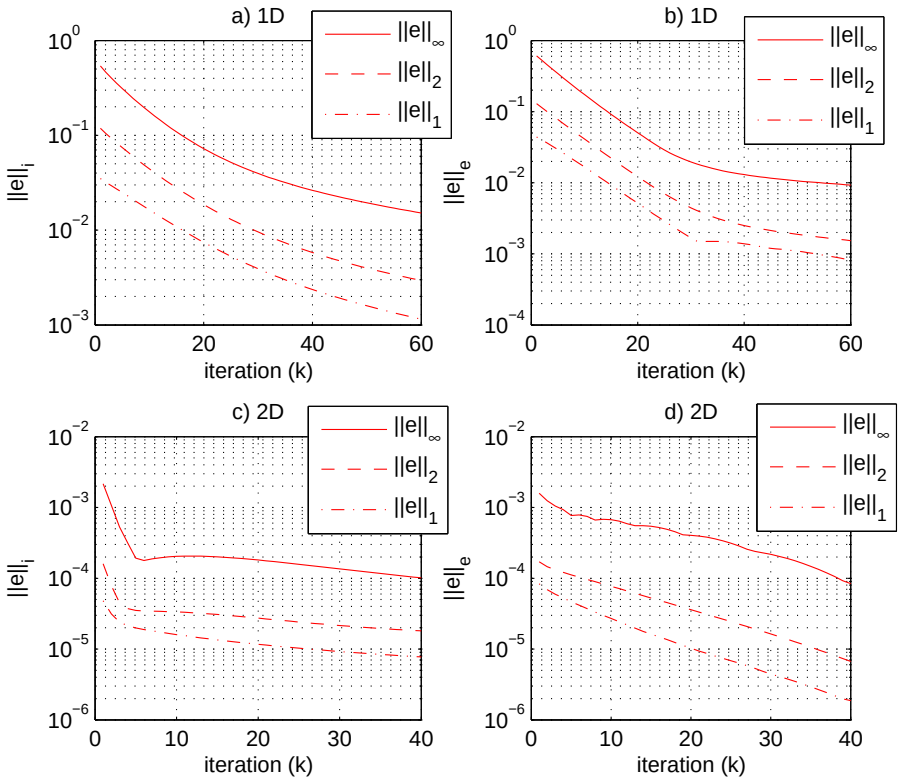

Figure 4.9: The errors iteration graph. (a) The errors for the ion density, (b) the errors for the electron density in one dimensional computations. (c) the ion density errors and (d) electron density errors.

The iteration error graphs for both computations are shown in (Figure 4.9). According to this figure, both numerical methods satisfy the convergence criteria. At the beginning of the

work, instead of the control volume approach the Taylor series approach is used in computations. Comparison between these two methods show that the control volume approach showed more proper convergence than the other method. Additionally, the computation of the stationary model showed weak convergence. It is observed that the computation of non-stationary equations yields more appropriate convergence. Moreover, in the process, the divergence is observed for $\theta < 0.5$ at the θ method and for the $\theta > 0.5$, which corresponds the strong implicit behavior, the convergence is more efficient for higher values.

It is observed that the usage of Gauss seidell and successive over relaxation scheme the value of the λ plays important role. For values $\lambda = 0.7 : 1 : 1.4 : 1.7$ the iteration numbers to converge the solution with a certain desired value of error are found as $iteration = 43 : 31 : 22 : 18$, where $\lambda < 1$ is under relaxation, $\lambda > 1$ is over relaxation with $\lambda = 1$ represents the Gauss Seidel method. For $\lambda = 2$, the numerical method diverged.

CHAPTER 5

CONCLUSION

We have developed self-consistent numerical model of DC driven glow discharge in argon. We used two-component plasma model based on the diffusion-drift theory and carried out the numerical investigation of the phenomena. The process at 1 t*orr* pressure, applied voltage of 350 V, the tube radius of 1.5 *cm* and 5 *cm* inter-electrode distance is analyzed. The computed results showed good qualitative agreement with the classical theory.

The voltage drop and cathode layer length relation shows resemblance with the experimental data. The cathode fall at the same applied voltage increased as the pressure raises and its strong resemblance with the corresponding Paschen curve is observed.

Different approximations for the ion mobility, ion diffusion and the ionization coefficient are analyzed. As a result, though mobility and diffusion parameters show resemblance, ionization coefficients yield significant differences, especially at the cathode layer. It is also observed that the recombination coefficient does not play significant role in the model.

The analysis of the convergence showed that the numerical method works properly. At the beginning of the process, instead of the control volume formulation, commonly used Taylor series method was employed and the comparison between them showed that the control volume approach is more efficient in the computation of this kind of equations. Besides, the non-uniform grid lowered the effectiveness and convergence enormously. The process of computation showed that the stationary equations, where the time dependence is eliminated, does not yield the proper convergence to the solution. Instead, the non-stationary equations with time dependence works appropriately in the process.

The computation in two dimension did not yield significant changes along radial direction, as

expected. It is observed that the iterative successive over relaxation lead convergence faster than the Gauss Seidell method. The raise in the successive over relaxation parameter ω up to 2 leads faster convergence though the values greater than this values showed divergence. The comparison of the method with the symmetric successive over relaxation may show further improvement on the computation.

REFERENCES

[1] Raizer Y. P.; *Gas Discharge Physics*, p. 1-378, Berlin: Springer-Verlag

[2] Llewellyn-Jones F.; *The Glow Discharge and an Introduction to Plasma Physics*, p. 1-23, New York: John Wiley & Sons (1966).

[3] Friedman A., Kennedy L.; *Plasma Physics and Engineering*, p. 204-505, New York: Taylor and Francis (2004).

[4] Chen F. F.; *Introduction to Plasma Physics and Controlled Fusion*, p. 53-285, New York: Plenum (1974).

[5] Boyd T. J. M., Sanderson J. J.; *The Physics of Plasmas*, p. 48-76, New York: Cambridge University (2003).

[6] Bellan P. M.; *Fundamentals of Plasma Physics*, p. 1-69, New York Cambridge University (2006).

[7] Goldston R. J., Rutherford P. H.; *Introduction to Plasma Physics*, p. 85-180, Bristol: IOP (1995).

[8] Lieberman M. A., Lichtenberg A. J.; *Principles of Plasma Discharges and Materials Processing*, p. 14-80, New Jersey: John Wiley & Sons (2005).

[9] Marcus R. K., Broekaert J. A. C.; *Glow Discharge Plasmas in Analytical Spectroscopy*, p.157, West Sussex: John Wiley & Sons (2003).

[10] Hoffman J. D.; *Numerical Methods for Egineers and Scientists*, p. 45-480, McGraw-Hill Inc. (1992)

[11] Ortega J. M., Rheinboldt W.S.; *Iterative Solution of Nonlinear Equations in Several Variables*, p. 180, New York: Siam (2000)

[12] Tveito A., Winther R.; *Inroduction to Partial Differential Equations: A Computational Approach*, p. 10-68, New York: Springer-Verlag (1998).

[13] Patankar S. V.; *Numerical Heat Transfer and Fluid Flow*, p.. 11-149, New York: Hemisphere (1980).

[14] Thomas J. W.; *Numerical Partial Differential Equations: Finite Difference Methods*, p. 10-139, New York: Springer-Verlag (1995).

[15] Thomas J. W.; *Numerical Partial Differential Equations: Conservation Laws and Elliptic Equations*, p. 51-392, New York: Springer-Verlag (1995).

[16] Wesseling P.; *Principles of Computational Fluid Dynamics*, p. 204, New York: Springer-Verlag (2000).

[17] Hundsdorfer W., Verwer J. G.; *Numerical Solution of Time-Dependent Advection-Diffusion-Reaction Equations*, p. 10-321, New York: Springer-Verlag (2003).

[18] Montijn C., Hundsdorfer W., Ebert U.; J. of Comp. Phys., 219, 801 (2006)

[19] Rafatov I. R., Akbar D., Bilikmen S.; Phys. Lett. A, 367, 114 (2007)

[20] Surzhikov T. S., Shang J. S.; J. of Comp. Phys, 199, 437 (2004)

[21] Ward A. L.; Phys. Rev., 6, 1852 (1958)

[22] Graves D. B., Jensen K. E. A.; IEEE Trans. Plasma Sci., PS-14, 2 (1986)

[23] Donkó Z., Hartmann P., Kutasi K.; Plasma Sources Sci. Technol., 15, 178 (2006)

[24] Ward A. L.; J. Appl. Phys., 33, 2789 (1962)

[25] Raizer Y. P., Surzhikov S. T.; High Temp., 26, 304 (1988)

[26] Raizer Y. P., Surzhikov S. T.; High Temp., 28, 324 (1990)

[27] Akbar D., Bilikmen S.; Chin. Phys. Lett., 23, 2498 (2006)

[28] Roy S., Pandey B. P., Poggie J., Gaitonde D. V.; Phys Plasmas, 10, 2578 (2003)

[29] Phelps A. V., Petrović Z. Lj.; Plasma Sources Sci. Technol., 8, R21 (1989)

[30] Marić D., Radmilović-Radenović M., Petrović Z. Lj.; Eur. Phys. J., D 35, 313 (2005)

[31] Grubert G. K., Loffhagen D., Uhrlandt D.; Two-fluid modelling of an abnormal low-pressure glow discharge, Proc. Femlab Conference 2005, 6 pp.

[32] Fiala A., Pitchford L. C., Boeuf J. P.; Phys. Rev. E, 49, 5607 (1994)

APPENDIX A

PROGRAMMING

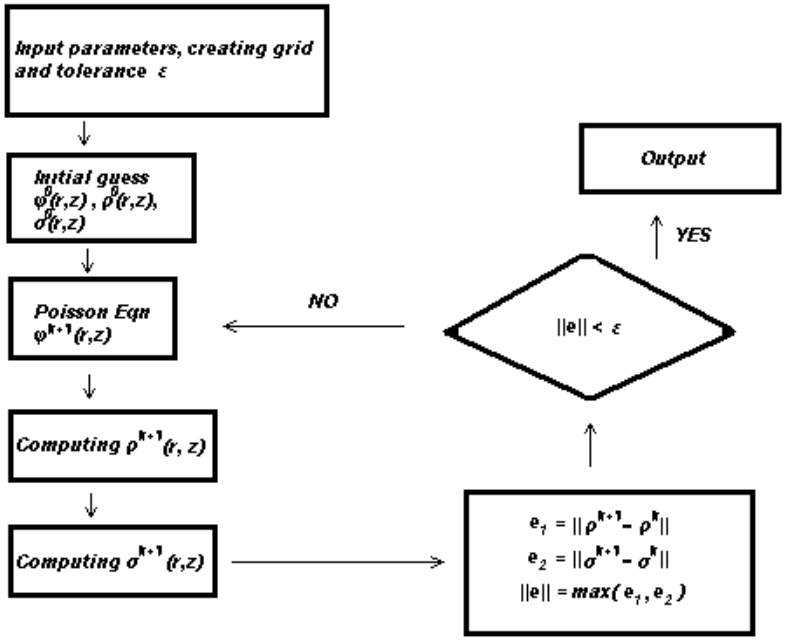

Figure A.1: The flow chart of the both programs.

The computations are processed in Matlab. Though the program has solvers for many kind of equations, for nonlinear problems they are absent. The flow chart of the both programs is shown in (Figure A.1).

A.1 One Dimensional Programming

One dimensional computing is processed via the m-files below. Operating main file is given first.

main

```
global N z zcv Lz p_Torr d_cm q_e ep_0 A B phi_V Td_Vcm2 Td n_cm3 n n_m3
global n1 Td_Vm2 Td1 ALPHA0 R0 E0 Ut n0 teta gamma
run set_constants
N=60;
[z,zcv]=grid(N,Lz);
load ni_dimensionless.txt;
load ne_dimensionless.txt;
z_=ni_dimensionless(:,1);
ni_=ni_dimensionless(:,2);
ne_=ne_dimensionless(:,2);
SIG=interp1(z_/max(z_),ne_,z/max(z));
RHO=interp1(z_/max(z_),ni_,z/max(z));
teta = .95;
tol =5e-3;
iteration = 1;

[Aa,Bb,Cc,Ff]=abcf(1,SIG,RHO,1,1) ;
V = tdma(Aa,Bb,Cc,Ff);
[Ecv] = efield(V);
[ E ] = ecv( Ecv );

while (ERROR>1),
    [dif1 con1]=di(2,E);
    delt1=timestep(dif1,con1);
    [dif2 con2]=di(3,E);
    delt2=timestep( dif2,con2);
    delt=.1*min(delt1,delt2);
    [Aa,Bb,Cc,Ff]=abcf(2,SIG,RHO,Ecv,E,delt);
    RHO1=tdma(Aa,Bb,Cc,Ff);
    [ERROR_RHO]=ERR(Aa,Bb,Cc,Ff,RHO,RHO1);
    [Aa,Bb,Cc,Ff]=abcf(3,SIG,RHO,Ecv,E,delt);
    SIG1=tdma(Aa,Bb,Cc,Ff);
    [ERROR_SIG]=ERR(Aa,Bb,Cc,Ff,SIG,SIG1);
    [Aa,Bb,Cc,Ff]=abcf(1,SIG1,RHO1,1,1,delt) ;
    V1=tdma(Aa,Bb,Cc,Ff);
    [Ecv1]=efield(V1);
    [E1]=ecv(Ecv1);
    k=iteration;
```

```
    iteration=iteration+1;
    [ERROR_RHO(4) ERROR_SIG(4)]
    ERROR = max(ERROR_RHO(3),ERROR_SIG(3));
    Ers_RHO_(1,k) =ERROR_RHO(3);
    Ers_RHO_(2,k) =ERROR_RHO(2);
    Ers_RHO_(3,k) =ERROR_RHO(1);
    Ers_RHO_(4,k) =ERROR_RHO(4);
    Ers_SIG_(1,k) =ERROR_SIG(3);
    Ers_SIG_(2,k) =ERROR_SIG(2);
    Ers_SIG_(3,k) =ERROR_SIG(1);
    Ers_SIG_(4,k) =ERROR_SIG(4);
    SIG=SIG1;
    RHO=RHO1;
    Ecv = Ecv1;
    E = E1;
    V = V1;
end
%-------------
```

grid

```
function [z,zcv] = grid(N,Lz)
for i = 1:N
    z(i) = grid_func(-5,i,N,0,Lz);
end
for i = 2:N
    zcv(i) = z(i-1) + (z(i) - z(i-1))/2 ;
end
 zcv(1) = -((z(2) - z(1))/2);
 zcv(N+1) = Lz + (z(N) - z(N-1))/2;
function [c]=grid_func(nu,numbers,n,a,b);
  if nu ~= 0
    c=a+(b-a)*(exp(nu*(numbers-1)/(n-1))-1)/(exp(nu)-1);
  else
    c=a+(b-a)*(numbers-1)/(n-1);
  end
%-------------
```

abcf

```
function [Aa,Bb,Cc,Ff]=abcf(a,SIG,RHO,Ecv,E,delt)
global N z zcv Lz p_Torr d_cm q_e ep_0 A B phi_V Td_Vcm2 Td n_cm3 n
global n_m3 n1 Td_Vm2 Td1 ALPHA0 R0 E0 Ut n0 teta gamma
Vx=-Ecv; Vxm=-E;
```

```
mu_e=3.0E5/p_Torr; Dif_SIG=3.0E5/p_Torr;
D_SIG=Dif_SIG/(R0*mu_e*E0)*ones(size(Ecv));
D_SIGm=Dif_SIG/(R0*mu_e*E0)*ones(size(E));
absE1=abs(Ecv*E0); En=absE1/n/Td;
mu_i1=(4.411e19./(1+(7.721e-3*En).^1.5).^0.33)/n;
Ep=abs(Ecv*E0/p_Torr); mu_ia=1.0E3*(1-2.22E-3*Ep)/p_Torr;
mu_ib=8.25E3*(Ep).^(-0.5).*(1-86.52*(Ep).^(-1.5))/p_Torr;
mu_i2=((mu_ia).*(Ep<=60) )+((mu_ib).*(Ep>60));
Dif_RHO1=0.025*mu_i1;
Dif_RHO2=2.0E2/p_Torr*ones(size(E)); D_RHO=Dif_RHO1/(R0*mu_e*E0);
mu=mu_i1/mu_e;
absE1=abs(E*E0); En2=1.0e2*absE1/n1/Td1; a1=(1.1e-22)*exp(-72./En2);
a2=(5.5e-21)*exp(-187./En2); a3=(3.2e-20)*exp(-700./En2);
a4=-(1.5e-20)*exp(-10000./En2); ALPHA2=(a1+a2+a3+a4)*n1*1.0e-2*R0;
En=absE1/n/Td;
ALPHA11=-2.748e-18*(En).^0.5+4.04e-19*(En)-7.40e-23*(En).^2;
ALPHA12=1.416e-23*(En).^3;
ALPHA1=n*R0*((ALPHA11).*(En>67.8)+(ALPHA12).*(En<=67.8));
SIGx(2:N-1)= (SIG(3:N)-SIG(1:N-2))./(z(3:N)-z(1:N-2));
SIGx(1)=(SIG(2)-SIG(1))/(z(2)-z(1));
SIGx(N)=(SIG(N)-SIG(N-1))/(z(N)-z(N-1));
beta_bar=2e-7; betta=ep_0*beta_bar/(q_e*mu_e);
absGAMMA=sqrt((D_SIGm.*SIGx-SIG.*Vxm).^2) ;
Ioniz=absGAMMA.*ALPHA1-betta*SIG.*RHO;
if a==1;
    Aa(1) = 0;
    Cc(N) = 0;
    Cc(1) = 0;
    Bb(1) = 1;
    Ff(1) = 0;
    Aa(N) = 0;
    Bb(N) = 1;
    Ff(N) = Ut;
    Aa(2:N-1) = 1./(z(2:N-1)-z(1:N-2));
    Bb(2:N-1) = (1./(z(3:N)-z(2:N-1))+1./(z(2:N-1)-z(1:N-2)));
    Cc(2:N-1) = 1./(z(3:N)-z(2:N-1));
    Ff(2:N-1) = (RHO(2:N-1)-SIG(2:N-1)).*(zcv(3:N)-zcv(2:N-1));
end
if a==2;
    Aa(1) = 0;
    Cc(N) = 0;
    Bb(1) = 1;
    Cc(1) = 0;
    Ff(1) = 0;
    Aa(N) = 1;
    Bb(N) = 1;
    Ff(N) = 0;
```

```
    Aa_(2:N-1)=delt*(max(-mu(2:N-1).*Vx(2:N-1),0)...
        +D_RHO(2:N-1)./(z(2:N-1)-z(1:N-2)));
    Aa(2:N-1)=teta*Aa_(2:N-1);
    Bb_(2:N-1)=delt*(max(-mu(3:N).*Vx(3:N),0)...
        +max(mu(2:N-1).*Vx(2:N-1),0)+D_RHO(3:N)./(z(3:N)-z(2:N-1))...
        +D_RHO(2:N-1)./(z(2:N-1)-z(1:N-2)));
    Bb(2:N-1)=teta*Bb_(2:N-1)+(zcv(3:N)-zcv(2:N-1));
    Cc_(2:N-1)= delt*( max(mu(3:N).*Vx(3:N),0 )...
        +D_RHO(3:N)./(z(3:N)-z(2:N-1)));
    Cc(2:N-1)=teta*Cc_(2:N-1);
    Ff(2:N-1)=delt*Ioniz(2:N-1).*(zcv(3:N)-zcv(2:N-1) ...
              -RHO(2:N-1).*((1-teta)*Bb_(2:N-1)-(zcv(3:N)-zcv(2:N-1)))...
              +RHO(3:N)*(1-teta).*Cc_(2:N-1) ...
              +RHO(1:N-2)*(1-teta).*Aa_(2:N-1);
end if a==3;
    Aa(1)=0;
    Cc(N)=0;
    Bb(1)=1;
    Cc(1)=1;
    Ff(1)=0;
    Bb(N)=1;
    Aa(N)=0;
    Ff(N)=gamma*mu(N)*RHO(N);
    Aa_(2:N-1)=delt*(max(Vx(2:N-1),0)...
        +D_SIG(2:N-1)./(z(2:N-1)-z(1:N-2)));
    Aa(2:N-1) =teta*Aa_(2:N-1);
    Bb_(2:N-1)=delt*(max(Vx(3:N),0)+max(-Vx(2:N-1),0)...
              +D_SIG(3:N)./(z(3:N)-z(2:N-1))...
              +D_SIG(2:N-1)./(z(2:N-1)-z(1:N-2)));
    Bb(2:N-1)=teta*Bb_(2:N-1) + (zcv(3:N)-zcv(2:N-1));
    Cc_(2:N-1)=delt*(max(-Vx(3:N),0 )+D_SIG(3:N)./(z(3:N)-z(2:N-1)));
    Cc(2:N-1) =teta*Cc_(2:N-1);
    Ff(2:N-1)=delt*Ioniz(2:N-1).*(zcv(3:N)-zcv(2:N-1))...
              -SIG(2:N-1).*((1-teta)*Bb_(2:N-1)-(zcv(3:N)-zcv(2:N-1)))...
              +SIG(3:N)*(1-teta).*Cc_(2:N-1)...
              +SIG(1:N-2)*(1-teta).*Aa_(2:N-1);
end
%-------------
```

tdma

```
function [f]=tdma(A,B,C,D);
  nn=length(A);
  p=zeros(1,nn);    q=zeros(1,nn);    f=zeros(1,nn);
  p(1)= C(1)/B(1);  q(1)=D(1)/B(1);
  for I = 2 : nn,
```

```
    rab=B(I)-A(I)*p(I-1);
    p(I)=C(I)/rab;
    q(I)=(D(I)+A(I)*q(I-1))/rab;
  end;
  f(nn)=q(nn);
  for I = (nn-1) : -1 : 1,
    f(I)=p(I)*f(I+1)+q(I);
  end
%-------------
```

ERR

```
function [ ERROR_ ] = ERR( Aa,Bb,Cc,Ff,PHI1,PHI,Delt )
global N z zcv Lz p_Torr d_cm q_e ep_0 A B phi_V Td_Vcm2 Td n_cm3 n
global n_m3 n1 Td_Vm2 Td1 ALPHA0 R0 E0 Ut n0 teta gamma
Ee_(1)=0; Ee_(N)=0;
Ee_(2:N-1)=-Aa(2:N-1).*PHI1(1:N-2)+Bb(2:N-1).*PHI1(2:N-1) ...
           -Cc(2:N-1).*PHI1(3:N) -Ff(2:N-1) ;
Ee=abs(Ee_);
del_z(1:N)=zcv(2:N+1)-zcv(1:N);
ERROR_one_=Ee.*del_z; ERROR_one=sum(ERROR_one_);
ERROR_two_=del_z.*Ee.^2; ERROR_two=sqrt(sum(ERROR_two_));
ERROR_inf=max(Ee);
ERROR_perc=100*max(abs((PHI1-PHI)))/max(PHI1);
ERROR_=[ERROR_one ERROR_two ERROR_inf ERROR_perc];
%-------------
```

timestep

```
function  delt  = timestep(  dif ,con )
global N z zcv Lz p_Torr d_cm q_e ep_0 A B phi_V Td_Vcm2 Td n_cm3 n
n_m3 global n1 Td_Vm2 Td1 ALPHA0 R0 E0 Ut n0 teta gamma
del_z(1:N)=zcv(2:N+1) - zcv(1:N);
delt_=abs(con./del_z) + 2*dif./(del_z.^2);
delt=(1/(1-teta))/max(delt_);
```

A.2 Two Dimensional Programming

Two dimensional computing is processed via the m-files below. Operating main file is given first.

main

```
global N M z zcv x xcv Lz Lx p_Torr d_cm q_e ep_0 A B phi_V Td_Vcm2
global Td n_cm3 n n_m3 n1 Td_Vm2 Td1 ALPHA0 R0 E0 Ut n0 teta gamma
run set_parameters
N = 60; M = 80; [z,zcv] = gridz(N,Lz); [x,xcv] = gridx(M,Lx);
load ni_dimensionless.txt; load ne_dimensionless.txt; load POT.txt;
load z_pot.txt; z_= ni_dimensionless(:,1);
ni_=ni_dimensionless(:,2); ne_= ne_dimensionless(:,2);
SIG1Dz=interp1(z_/max(z_),ne_,z/max(z));
RHO1Dz=interp1(z_/max(z_),ni_,z/max(z));
PHI1Dz=interp1(z_pot/max(z_pot),POT,z/max(z));
for i=1:1:N;
    for j=1:1:M;
        SIG(i,j) = SIG1Dz(i);
        RHO(i,j) = RHO1Dz(i);
        PHI(i,j) = PHI1Dz(i);
    end
end
tol=10^-4; omega=.7; teta = .85; efe0= 0.95; ERROR=1;
Ers_RHO=zeros(4,10); Ers_SIG=zeros(4,10); err=1; iter=0;
while (ERROR>tol),
    iter= iter+1;
    [ Aa,Bb,Cc,Dd,Ee,Ff ] = potentialabcdef( RHO-SIG );
    err_phi= 1;
    iter_phi= 1;
    while ((err_phi>0.00001)&(iter_phi<5000)),
        PHI1 = gauss_seidellsor(1,Aa,Bb,Cc,Dd,Ee,Ff,PHI,0,0,omega);
        PHI=efe0*PHI1+ (1-efe0)*PHI;
        err_phi= 100*max(max(abs( (PHI-PHI1))))/max(max(abs(PHI)));
        iter_phi= iter_phi+1;
    end
    disp('\phi');
    [iter err_phi iter_phi]
    [ Ex_zxcv, Ez_zcvx ] = efielda( PHI1 );
    [ E,Ex,Ez,Ex_zcvx,Ez_zxcv ] = efieldb( Ex_zxcv, Ez_zcvx );
    [Di_RHO, absC_RHO] = diabsc(2,E);
    delt_RHO  = timestep(  Di_RHO ,absC_RHO );
    Delt=.001;
    err_rho= 1;
    iter_rho= 1;
    while ((err_rho>0.001)&(iter_rho<1000)),
        [Dzxcv,Dzcvx,uzxcv,uzcvx,vzxcv,vzcvx,S,mu  ] =...
            dicos(2,RHO,SIG,Ex_zcvx,Ez_zxcv,Ex_zxcv, Ez_zcvx,Ex,Ez);
        [Aa,Bb,Cc,Dd,Ee,Ff] =...
            abcdef(Dzxcv,Dzcvx,uzxcv,uzcvx,vzxcv,vzcvx,S,Delt,RHO );
        RHO1 = gauss_seidellsor(2,Aa,Bb,Cc,Dd,Ee,Ff,RHO,mu,RHO,omega);
        err_rho= 100*max(max(abs(  (RHO-RHO1))))/max(max(abs(RHO)));
        iter_rho= iter_rho+1;
```

```
        RHO_iterative =RHO;
        RHO = RHO1;
    end
    [ Err_RHO_ ] = ERR( Aa,Bb,Cc,Dd,Ee,Ff,RHO_iterative,RHO1,Delt );
    Err_RHO(1,iter)= Err_RHO_(1);
    Err_RHO(2,iter)= Err_RHO_(2);
    Err_RHO(3,iter)= Err_RHO_(3);
    Err_RHO(4,iter)= Err_RHO_(4);
    ERROR1 = Err_RHO_(3);
    err_sig= 1;
    iter_sig= 1;
    while ((err_sig>0.001)&(iter_sig<100)),
        [Dzxcv,Dzcvx,uzxcv,uzcvx,vzxcv,vzcvx,S,mu  ] = ...
            dicos(3,RHO,SIG,Ex_zcvx,Ez_zxcv,Ex_zxcv, Ez_zcvx,Ex,Ez);
        [ Aa,Bb,Cc,Dd,Ee,Ff ] =...
            abcdef( Dzxcv,Dzcvx,uzxcv,uzcvx,vzxcv,vzcvx,S,Delt,SIG );
        SIG1 = gauss_seidellsor(3,Aa,Bb,Cc,Dd,Ee,Ff,SIG,mu,RHO,omega);
        err_sig= 100*max(max(abs(  (SIG-SIG1))))/max(max(abs(SIG)));
        iter_sig= iter_sig+1;
        SIG_iterative =SIG;
        SIG =SIG1;
    end
    [iter err_sig iter_sig err_rho iter_rho ]
    [ Err_SIG_ ] = ERR( Aa,Bb,Cc,Dd,Ee,Ff,SIG_iterative,SIG1,Delt );
    Err_SIG(1,iter)= Err_SIG_(1);
    Err_SIG(2,iter)= Err_SIG_(2);
    Err_SIG(3,iter)= Err_SIG_(3);
    Err_SIG(4,iter)= Err_SIG_(4);
    err= max(err_sig,err_rho);
    ERROR2 = Err_SIG_(3);
    ERROR = max(ERROR1, ERROR2);
end
%-------------
```

gridz

```
function [z,zcv] = gridz(N,Lz)
for i = 1:N
    z(i) = grid_func(-5,i,N,0,Lz);
end
for i = 2:N
    zcv(i) = z(i-1) + (z(i) - z(i-1))/2 ;
end
 zcv(1) = -((z(2) - z(1))/2);
 zcv(N+1) = Lz + (z(N) - z(N-1))/2;
function [c]=grid_func(nu,numbers,n,a,b);
```

```
  if nu ~= 0
    c=a+(b-a)*(exp(nu*(numbers-1)/(n-1))-1)/(exp(nu)-1);
  else
    c=a+(b-a)*(numbers-1)/(n-1);
  end
%-------------
```

gridx

```
function [z,zcv] = gridx(N,Lz)
for i = 1:N
    z(i) = grid_func(3,i,N,0,Lz);
end
for i = 2:N
    zcv(i) = z(i-1) + (z(i) - z(i-1))/2 ;
end
 zcv(1) = -((z(2) - z(1))/2);
 zcv(N+1) = Lz + (z(N) - z(N-1))/2;
function [c]=grid_func(nu,numbers,n,a,b);
  if nu ~= 0
    c=a+(b-a)*(exp(nu*(numbers-1)/(n-1))-1)/(exp(nu)-1);
  else
    c=a+(b-a)*(numbers-1)/(n-1);
  end
%-------------
```

potentialabcdef

```
function [ Aa,Bb,Cc,Dd,Ee,Ff ] = potentialabcdef( S )
global N M z zcv x xcv Lz Lx p_Torr d_cm q_e ep_0 A B phi_V Td_Vcm2
global Td n_cm3 n n_m3 n1 Td_Vm2 Td1 ALPHA0 R0 E0 Ut n0 teta gamma
Delz(1:N)=zcv(2:N+1)-zcv(1:N); Delx(1:M)=xcv(2:M+1)-xcv(1:M);
Aa=zeros(N,M); Bb=zeros(N,M); Cc=zeros(N,M); Dd=zeros(N,M);
Ee=zeros(N,M); Ff=zeros(N,M);
for i = 2:N-1;
    for j = 2:M-1;
        Aa(i,j) = xcv(j+1)*Delz(i)/(x(j+1) - x(j));
        Bb(i,j) = x(j)*Delx(j)/(z(i+1) - z(i));
        Cc(i,j) = xcv(j+1)*Delz(i)/(x(j+1) - x(j)) ...
                  + xcv(j)*Delz(i)/(x(j) - x(j-1)) ...
                  + x(j)*Delx(j)/(z(i+1) - z(i)) ...
                  + x(j)*Delx(j)/(z(i) - z(i-1));
        Dd(i,j) = xcv(j)*Delz(i)/(x(j)-x(j-1));
        Ee(i,j) = x(j)*Delx(j)/(z(i) - z(i-1));
```

```
        Ff(i,j) = S(i,j)*x(j)*Delx(j)*Delz(i);
    end
end
%-------------
```

gauss_seidellsor

```
function [eta]=gauss_seidellsor(a,
Aa,Bb,Cc,Dd,Ee,Ff,eta1,mu,RHO,omega)
global N M z zcv x xcv Lz Lx p_Torr d_cm q_e ep_0 A B phi_V Td_Vcm2
global Td n_cm3 n n_m3 n1 Td_Vm2 Td1 ALPHA0 R0 E0 Ut n0 teta gamma
etaa=eta1;
for i = 2:1:N-1;
    for j=2:1:M-1;

        eta1(i,j) = (   Aa(i,j)*eta1(i,j+1) + Bb(i,j)*eta1(i+1,j) ...
                    + Dd(i,j)*eta1(i,j-1) + Ee(i,j)*eta1(i-1,j) ...
                    +Ff(i,j) )/Cc(i,j);
    end
end
eta1=omega*eta1 +(1-omega)*etaa;
if a==1;
    for j=1:1:M;
        eta1(1,j)=0;
        eta1(N,j)=Ut;
    end
    for i=1:1:N;
        eta1(i,1)=eta1(i,2);
        eta1(i,M)=eta1(i,M-1);
    end
end
if a==2;
    for j=1:1:M;
        eta1(1,j)=0;
        eta1(N,j)=eta1(N-1,j);
    end
    for i=1:1:N;
        eta1(i,1)=eta1(i,2);
        eta1(i,M)=eta1(i,M-1);
    end
end
if a==3;
    for j=1:1:M
        eta1(1,j) = eta1(2,j);
        eta1(N,j) = gamma*mu(N,j)*RHO(N,j);
    end
```

```
    for i=1:1:N;
        eta1(i,1)=eta1(i,2);
        eta1(i,M)=eta1(i,M-1);
    end
end
eta = eta1 ;
%-------------
```

efielda

```
function [ uzxcv, vzcvx ] = efielda( phi )
global N M z zcv x xcv Lz Lx p_Torr d_cm q_e ep_0 A B phi_V Td_Vcm2
global Td n_cm3 n n_m3 n1 Td_Vm2 Td1 ALPHA0 R0 E0 Ut n0 teta gamma
%u = Ex =Er
%v = Ez
for i = 2:1:N;
    for j = 1:1:M;
        vzcvx(i,j) = -(phi(i,j) - phi(i-1,j))/(z(i)-z(i-1));
        vzcvx(1,j) = 0;
        vzcvx(N+1,j) = 0;
    end
end
for i = 1:1:N;
    for j = 2:1:M;
        uzxcv(i,j) = -(phi(i,j) - phi(i,j-1))/(x(j)-x(j-1));
        uzxcv(i,1) = 0;
        uzxcv(i,M+1) = 0;
    end
end
%-------------
```

efieldb

```
function [ E,u,v,uzcvx,vzxcv ] = efieldb( uzxcv, vzcvx )
global N M z zcv x xcv Lz Lx p_Torr d_cm q_e ep_0 A B phi_V Td_Vcm2
global Td n_cm3 n n_m3 n1 Td_Vm2 Td1 ALPHA0 R0 E0 Ut n0 teta gamma
for i=1:1:N;
    for j=2:1:M-1;
        u1(i,j) = uzxcv(i,j)...
            +(x(j)-xcv(j))*(uzxcv(i,j+1)-uzxcv(i,j))/(xcv(j+1)-xcv(j));
    end
end
for i=1:1:N;
    u1(i,1) = uzxcv(i,2)...
```

```
        -(xcv(2)-x(1))*(u1(i,2)-uzxcv(i,2))/(x(2)-xcv(2));
    u1(i,M) = uzxcv(i,M)...
        +(x(M)-xcv(M))*(uzxcv(i,M)-u1(i,M-1))/(xcv(M)-x(M-1));
end
u=u1;
for j=1:1:M;
    for i=2:1:N-1;
        v1(i,j) = vzcvx(i,j)...
            +(z(i)-zcv(i))*(vzcvx(i+1,j)-vzcvx(i,j))/(zcv(i+1)-zcv(i));
    end
end
for j=1:1:M;
    v1(1,j) = vzcvx(2,j)...
        -(zcv(2)-z(1))*(v1(2,j)-vzcvx(2,j))/(z(2)-zcv(2));
    v1(N,j) = vzcvx(N,j)...
        +(z(N)-zcv(N))*(vzcvx(N,j)-v1(N-1,j))/(zcv(N)-z(N-1));
end
v=v1;
for i=2:1:N;
    for j=1:1:M;
        u1zcvx(i,j) = u(i,j)...
            - (z(i)-zcv(i))*(u(i,j)-u(i-1,j))/(z(i)-z(i-1));
    end
end
for j=1:1:M;
    u1zcvx(1,j) = 0;
    u1zcvx(N+1,j) = 0;
end
uzcvx=u1zcvx;
for j=2:1:M;
    for i=1:1:N;
        v1zxcv(i,j) = v(i,j)...
            - (x(j)-xcv(j))*(v(i,j)-v(i,j-1))/(x(j)-x(j-1));
    end
end
for i=1:1:N;
    v1zxcv(i,1) = 0;
    v1zxcv(i,M+1) =0;
end
vzxcv=v1zxcv; for i=1:1:N;
    for j=1:1:M;
        E(i,j) = sqrt(u(i,j)^2 +v(i,j)^2);
    end
end
%-------------
```

diabsc

```
function [ D,absC ] = diabsc( nu,E )
global N M z zcv x xcv Lz Lx p_Torr d_cm q_e ep_0 A B phi_V Td_Vcm2
global Td n_cm3 n n_m3 n1 Td_Vm2 Td1 ALPHA0 R0 E0 Ut n0 teta gamma
mu_e=3.0E5/p_Torr; Dif_SIG=3.0E5/p_Torr;
D_SIG=Dif_SIG/(R0*mu_e*E0)*ones(size(E));
absE1=abs(E*E0); En=absE1/n/Td;
mu_i1=(4.411e19./(1+(7.721e-3*En).^1.5).^0.33)/n;
Ep=abs(E*E0/p_Torr); mu_ia=1.0E3*(1-2.22E-3*Ep)/p_Torr;
mu_ib=8.25E3*(Ep).^(-0.5).*(1-86.52*(Ep).^(-1.5))/p_Torr;
mu_i2=((mu_ia).*(Ep<=60) )+((mu_ib).*(Ep>60));
Dif_RHO1=0.025*mu_i1; Dif_RHO2=ones(size(E))*2.0E2/p_Torr ;
D_RHO=Dif_RHO1/(R0*mu_e*E0);
mu=mu_i1/mu_e;
if nu==2;
    absC =mu.*E;
    D = D_RHO;
end
if nu==3;
    absC =E;
    D = D_SIG;
end
%-------------
```

dicos

```
function [Dzxcv,Dzcvx,uzxcv,uzcvx,vzxcv,vzcvx,S,mu  ] =...
    dicos(nu,RHO,SIG,Ex_zcvx,Ez_zxcv,Ex_zxcv, Ez_zcvx,Ex,Ez)
global N M z zcv x xcv Lz Lx p_Torr d_cm q_e ep_0 A B phi_V Td_Vcm2
global Td n_cm3 n n_m3 n1 Td_Vm2 Td1 ALPHA0 R0 E0 Ut n0 teta gamma
for i = 1:1:N+1;
    for j=1:1:M;
        E_zcvx(i,j) = sqrt( Ex_zcvx(i,j)^2 + Ez_zcvx(i,j)^2  );
    end
end
for i=1:1:N;
    for j=1:1:M+1
        E_zxcv(i,j) = sqrt( Ex_zxcv(i,j)^2 + Ez_zxcv(i,j)^2  );
    end
end
for i=1:1:N;
    for j=1:1:M;
        E(i,j) = sqrt( Ex(i,j)^2 + Ez(i,j)^2 );
    end
```

```
end
run set_expressions
for i=2:1:N-1;
    for j=2:1:M-1;
        SIGz(i,j) = (SIG(i+1,j) - SIG(i-1,j))/(z(i+1)-z(i-1));
        SIGx(i,j) = (SIG(i,j+1) - SIG(i,j-1))/(x(j+1)-x(j-1));
    end
end
for j=1:1:M;
    SIGz(1,j) = (SIG(2,j)-SIG(1,j))/(z(2)-z(1));
    SIGz(N,j) = (SIG(N,j)-SIG(N-1,j))/(z(N)-z(N-1));
end
for i=1:1:N
    SIGx(i,1) = (SIG(i,2)-SIG(i,1))/(x(2)-x(1));
    SIGx(i,M) = (SIG(i,M)-SIG(i,M-1))/(x(M)-x(M-1));
end
beta_bar = 2e-7; beta = ep_0*beta_bar/(q_e*mu_e);
absGAMMA=sqrt((D_SIGm.*SIGx+SIG.*Ex).^2+(D_SIGm.*SIGz+SIG.*Ez).^2);
Ioniz=absGAMMA.*ALPHA1 -beta*SIG.*RHO;
if nu==2;
    uzxcv = mu_zxcv.*Ex_zxcv;
    uzcvx = mu_zcvx.*Ex_zcvx;
    vzxcv = mu_zxcv.*Ez_zxcv;
    vzcvx = mu_zcvx.*Ez_zcvx;
    Dzxcv = D_RHO_zxcv;
    Dzcvx = D_RHO_zcvx;
    S = Ioniz;
end
if nu==3;
    uzxcv = -Ex_zxcv;
    uzcvx = -Ex_zcvx;
    vzxcv = -Ez_zxcv;
    vzcvx = -Ez_zcvx;
    Dzxcv = D_SIG_zxcv;
    Dzcvx = D_SIG_zcvx;
    S = Ioniz;
end
%-------------
```

set_expressions

```
Vxm = -E;
mu_e=3.0E5/p_Torr; Dif_SIG=3.0E5/p_Torr;
D_SIG_zcvx=Dif_SIG/(R0*mu_e*E0)*ones(size(E_zcvx));
D_SIG_zxcv=Dif_SIG/(R0*mu_e*E0)*ones(size(E_zxcv));
D_SIGm=Dif_SIG/(R0*mu_e*E0)*ones(size(E));
```

```
absE1_zcvx=abs(E_zcvx*E0); En_zcvx=absE1_zcvx/n/Td;
mu_i1_zcvx=(4.411e19./(1+(7.721e-3*En_zcvx).^1.5).^0.33)/n;
Ep_zcvx=abs(E_zcvx*E0/p_Torr);
mu_ia_zcvx=1.0E3*(1-2.22E-3*Ep_zcvx)/p_Torr;
mu_ib_zcvx=8.25E3*(Ep_zcvx).^(-0.5).*(1-86.52*(Ep_zcvx).^(-1.5))/p_Torr;
mu_i2_zcvx=((mu_ia_zcvx).*(Ep_zcvx<=60))+((mu_ib_zcvx).*(Ep_zcvx>60));
Dif_RHO1_zcvx=0.025*mu_i1_zcvx;
Dif_RHO2_zcvx=ones(size(E_zcvx))*2.0E2/p_Torr;
D_RHO_zcvx=Dif_RHO1_zcvx/(R0*mu_e*E0);
mu_zcvx=mu_i1_zcvx/mu_e;
absE1_zxcv=abs(E_zxcv*E0); En_zxcv=absE1_zxcv/n/Td;
mu_i1_zxcv=(4.411e19./(1+(7.721e-3*En_zxcv).^1.5).^0.33)/n;
Ep_zxcv=abs(E_zxcv*E0/p_Torr);
mu_ia_zxcv=1.0E3*(1-2.22E-3*Ep_zxcv)/p_Torr;
mu_ib_zxcv=8.25E3*(Ep_zxcv).^(-0.5).*(1-86.52*(Ep_zxcv).^(-1.5))/p_Torr;
mu_i2_zxcv=((mu_ia_zxcv).*(Ep_zxcv<=60))+((mu_ib_zxcv).*(Ep_zxcv>60));
Dif_RHO1_zxcv=0.025*mu_i1_zxcv;
Dif_RHO2_zxcv=ones(size(E_zxcv))*2.0E2/p_Torr;
D_RHO_zxcv=Dif_RHO1_zxcv/(R0*mu_e*E0);
mu_zxcv=mu_i1_zxcv/mu_e;
absE1=abs(E*E0); En=absE1/n/Td;
mu_i1=(4.411e19./(1+(7.721e-3*En).^1.5).^0.33)/n;
Ep=abs(E*E0/p_Torr); mu_ia= 1.0E3*(1-2.22E-3*Ep)/p_Torr;
mu_ib=8.25E3*(Ep).^(-0.5).*(1-86.52*(Ep).^(-1.5))/p_Torr;
mu_i2=((mu_ia).*(Ep<=60) )+((mu_ib).*(Ep>60));
Dif_RHO1=0.025*mu_i1; Dif_RHO2=ones(size(E))*2.0E2/p_Torr;
D_RHO=Dif_RHO1/(R0*mu_e*E0);
mu=mu_i1/mu_e;
absE1=abs(E*E0); En2=1.0e2*absE1/n1/Td1; a1=(1.1e-22)*exp(-72./En2);
a2=(5.5e-21)*exp(-187./En2); a3=(3.2e-20)*exp(-700./En2);
a4=-(1.5e-20)*exp(-10000./En2); ALPHA2=(a1+a2+a3+a4)*n1*1.0e-2*R0;
En=absE1/n/Td;
ALPHA11=-2.748e-18*(En).^0.5+4.04e-19*(En)-7.40e-23*(En).^2;
ALPHA12=1.416e-23*(En).^3;
ALPHA1=n*R0*((ALPHA11).*(En>67.8)+(ALPHA12).*(En<=67.8));
%-------------
```

abcdef

```
function
[Aa,Bb,Cc,Dd,Ee,Ff]=abcdef(Dzxcv,Dzcvx,uzxcv,uzcvx,vzxcv,vzcvx,S,Delt,eta1)
global N M z zcv x xcv Lz Lx p_Torr d_cm q_e ep_0 A B phi_V Td_Vcm2
global Td n_cm3 n n_m3 n1 Td_Vm2 Td1 ALPHA0 R0 E0 Ut n0 teta gamma
Delz(1:N) = zcv(2:N+1) - zcv(1:N); Delx(1:M) = xcv(2:M+1) -
xcv(1:M); Aa = zeros(N,M); Bb = zeros(N,M); Cc = zeros(N,M); Dd =
zeros(N,M); Ee = zeros(N,M); Ff = zeros(N,M);
```

```
for i=2:1:N-1;
    for j=2:1:M-1;
        Aa_(i,j) = Dzxcv(i,j+1)*xcv(j+1)*Delz(i)/(x(j+1)-x(j)) ...
                  +xcv(j+1)*max(-uzxcv(i,j+1),0)*Delz(i) ;
        Aa = Delt*teta*Aa_;
        Bb_(i,j) = Dzcvx(i+1,j)*x(j)*Delx(j)/(z(i+1) - z(i)) ...
                  +max(-vzcvx(i+1,j),0)*x(j)*Delx(j);
        Bb =  Delt*teta*Bb_;
        Cc_(i,j) = Dzxcv(i,j+1)*xcv(j+1)*Delz(i)/(x(j+1) - x(j)) ...
                  +Dzxcv(i,j)*xcv(j)*Delz(i)/(x(j) - x(j-1)) ...
                  +Dzcvx(i+1,j)*x(j)*Delx(j)/(z(i+1) - z(i)) ...
                  +Dzcvx(i,j)*x(j)*Delx(j)/(z(i)-z(i-1)) ...
                  +xcv(j+1)*max(uzxcv(i,j+1),0)*Delz(i) ...
                  +xcv(j)*max(-uzxcv(i,j),0)*Delz(i) ...
                  +max(vzcvx(i+1,j),0)*x(j)*Delx(j) ...
                  +max(-vzcvx(i,j),0)*x(j)*Delx(j);
        Cc(i,j) = Delt*teta*Cc_(i,j) + x(j)*Delx(j)*Delz(i);
        Dd_(i,j) = Dzxcv(i,j)*xcv(j)*Delz(i)/(x(j)-x(j-1)) ...
                  +xcv(j)*max(uzxcv(i,j),0)*Delz(i);
        Dd = Delt*teta*Dd_;
        Ee_(i,j) = Dzcvx(i,j)*x(j)*Delx(j)/(z(i)-z(i-1)) ...
                  +max(vzcvx(i,j),0)*x(j)*Delx(j);
        Ee = Delt*teta*Ee_;
        Ff_(i,j) = S(i,j)*x(j)*Delx(j)*Delz(i) ...
                   +(1-teta)*( Aa_(i,j)*eta1(i,j+1) ...
                   +Bb_(i,j)*eta1(i+1,j) - Cc_(i,j)*eta1(i,j) ...
                   + Dd_(i,j)*eta1(i,j-1) + Ee_(i,j)*eta1(i-1,j));
        Ff(i,j) = Delt*Ff_(i,j) +x(j)*Delx(j)*Delz(i)*eta1(i,j);
    end
end
%-------------
```

ERR

```
function [ ERROR_ ] = ERR( Aa,Bb,Cc,Dd,Ee,Ff,PHI,PHI1,Delt )
global N M z zcv x xcv Lz Lx p_Torr d_cm q_e ep_0 A B phi_V Td_Vcm2
global Td n_cm3 n n_m3 n1 Td_Vm2 Td1 ALPHA0 R0 E0 Ut n0 teta gamma
Delz(1:N)=zcv(2:N+1)-zcv(1:N); Delx(1:M)=xcv(2:M+1)-xcv(1:M);
for i=1:1:N;
    Er_(i,1)=0;
    Er_(i,M)=0;
end
for j=1:1:M;
    Er_(1,j)=0;
    Er_(N,j)=0;
end
```

```
for i=2:1:N-1;
    for j=2:1:M-1;
      Er_(i,j) =Cc(i,j)*PHI(i,j)-Aa(i,j)*PHI(i,j+1)...
          -Bb(i,j)*PHI(i+1,j-Dd(i,j)*PHI(i,j-1)...
          -Ee(i,j)*PHI(i-1,j)-Ff(i,j);
    end
end
Er = abs(Er_);
for i=1:N;
    for j=1:M;
        ERROR_one_(i,j)=Er(i,j)*Delz(i)*Delx(j);
    end
end
ERROR_one = sum(sum(ERROR_one_));
for i=1:N;
    for j=1:M;
    ERROR_two_(i,j) = Delz(i)*Delx(j)*Er(i,j)^2;
    end
end
ERROR_two = sqrt(sum(sum(ERROR_two_)));
ERROR_inf = max(max(Er));
ERROR_perc= 100*max(max(abs(  (PHI1-PHI))))/max(max(abs(PHI1)));
ERROR_ = [ERROR_one ERROR_two ERROR_inf ERROR_perc];
%-------------
```